

Charge glass in an extended dimer Hubbard model

Meldon B. Deglint,¹ Krishant Akella,² and Malcolm P. Kennett²

¹*Department of Geoscience, University of Calgary, Calgary, Alberta T2N 1N4, Canada*

²*Department of Physics, Simon Fraser University, Burnaby, British Columbia V5A 1S6, Canada*



(Received 4 October 2021; revised 13 May 2022; accepted 4 August 2022; published 15 August 2022)

The charge degrees of freedom in several different organic charge transfer salts display slow or glassy dynamics. To gain insight into this behavior, we obtain the low-energy theory for an extended dimer Hubbard model, considering the occupations of sites on neighboring dimers. We take a classical limit of the resulting effective model of coupled spins and dimers and study it using classical Monte Carlo simulations. We find that frustration induced by intradimer and interdimer interactions leads to glassiness in the charge degrees of freedom in the absence of ordering of the spin degrees of freedom. Our results may have relevance to experimental observations of relaxor ferroelectric behavior in the dynamics of organic charge transfer salts.

DOI: [10.1103/PhysRevB.106.085123](https://doi.org/10.1103/PhysRevB.106.085123)

I. INTRODUCTION

Strong interactions between charge and spin degrees of freedom are responsible for numerous phases in strongly correlated electron materials. One particularly attractive class of materials for investigating such effects are organic charge transfer salts [1–3]. These materials display phenomena such as unconventional superconductivity and spin liquid behavior [4,5].

In addition to low-temperature phenomena, at temperatures on the order of tens of kelvins, slow and glassy charge dynamics have been observed, particularly in the dielectric relaxation of the κ -(BEDT-TTF)₂X family of organic charge transfer salts [6,7]. In the organic charge transfer salt κ -(BEDT-TTF)₂Cu₂(CN)₃, which shows spin-liquid behavior at low temperatures, there is broad in-plane dielectric relaxation and out-of-plane relaxorlike dielectric response below ~ 60 K [8]. A glassy response has also been observed in the dielectric function of κ -(BEDT-TTF)₂Ag₂(CN)₃ [9], and glassy freezing of electrons at low temperatures has been suggested for κ -(BEDT-TTF)₂Hg(SCN)₂Br [10].

The origin of the electric dipoles that give rise to the relaxor ferroelectric behavior in κ -(BEDT-TTF)₂X salts is still an active area of investigation. There is evidence for charge disproportionation in dimers in κ -(BEDT-TTF)₂Hg(SCN)₂Cl [11] but Sedlmeier *et al.* [12] did not find evidence for charge disproportionation in κ -(BEDT-TTF)₂Cu₂(CN)₃, κ -(BEDT-TTF)₂Cu[N(CN)₂]Cl, or κ -(BEDT-TTF)₂Cu[N(CN)₂]Br. Pinterić *et al.* [13] have argued that optical measurements of κ -(BEDT-TTF)₂Cu₂(CN)₃ are not consistent with local dipoles. Suggested mechanisms for glassy dynamics that do not involve dipoles in dimers include domain walls between dimer Mott and charge-ordered phases [14] and a dielectric catastrophe [15]. At higher temperatures, disorder in the conformational orientation of ethylene groups in

BEDT-TTF [16] has been implicated in glassy dynamics in κ -(BEDT-TTF)₂X materials [17,18].

Relaxor ferroelectric or glassy behavior has also been seen in several other families of organic charge transfer salts, such as β' -Pd(dmit)₂ salts [19,20], β' -(BEDT-TTF)₂ICl₂ [21,22], θ -(BEDT-TTF)₂RbZn(SCN)₄ [23], and θ -(BEDT-TTF)₂CsZn(SCN)₄ [24,25], usually in the tens of kelvin temperature range. A dielectric peak like those seen in relaxor ferroelectrics is also seen in α -(BEDT-TTF)₂I₃ [26,27].

Many of the κ -(BEDT-TTF)₂X salts such as κ -(BEDT-TTF)₂Cu₂(CN)₃ can be described by a triangular lattice of dimers forming a quarter-filled extended two-dimensional Hubbard model with both intradimer and interdimer interactions [28–30]. Quarter-filled extended Hubbard models have been identified as enhancing geometric frustration of charge degrees of freedom [31], and geometric frustration in charge ordering has been emphasized as a factor in leading to a charge cluster glass with no long-range order in θ -(BEDT-TTF)₂RbZn(SCN)₄ [23].

In this paper, we study a quarter-filled extended dimer Hubbard model with the same form as that proposed to describe κ -(BEDT-TTF)₂Cu₂(CN)₃. Following Ref. [28], we obtain the low-energy theory in the one electron per dimer limit, which can be written in terms of spin and dipole degrees of freedom. Going beyond Ref. [28], we consider the occupation of next-nearest neighbor sites on the couplings in the effective Hamiltonian as was done for an extended Hubbard model on a square lattice [32,33]. This leads to a distribution of couplings between spin and dipole degrees of freedom in the low-energy theory. Rather than simulate the resulting model directly, which would be prohibitively computationally expensive, we make a classical approximation, which gives a model of vector spins coupled to Ising dipoles and study this model with classical Monte Carlo simulations. Our main result is that, in

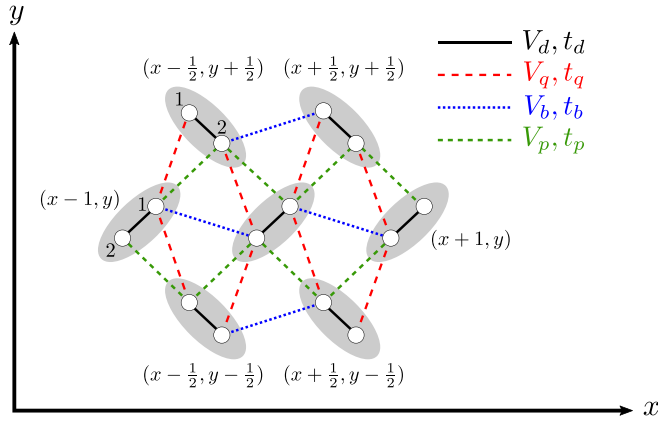


FIG. 1. Triangular lattice of dimers used for the extended Hubbard model. The position of the central dimer is (x, y) . The t_i denote different types of hopping, and the V_i denote nearest neighbor interactions.

this approximate model, we find that glassiness in the charge degrees of freedom occurs over a range of intradimer and interdimer nearest neighbor interaction strengths. While the classical approximation is uncontrolled, it should be viewed in the same spirit as mean field theory—our calculation demonstrates the potential for glassiness in the system.

This paper is structured as follows: in Sec. II, we introduce the model we study and describe how we obtain the low-energy theory. In Sec. III, we discuss our Monte Carlo simulations of the simplified model and the results we obtain from our simulations. Finally, in Sec. IV, we discuss our results and conclude.

II. MODEL

We consider a two-dimensional extended Hubbard model of dimers on a triangular lattice, introduced by Hotta [28] for κ -(BEDT-TTF)₂Cu₂(CN)₃. We allow for both intradimer and interdimer hopping, onsite interactions, and both intradimer and interdimer nearest neighbor interactions. All hops and interactions are illustrated in Fig. 1. We write the Hamiltonian as

$$H = H_T + H_U + H_V, \quad (1)$$

where H_T is the hopping part of the Hamiltonian, H_U is the onsite Hubbard interaction, and H_V is the nearest neighbor interaction term. We now consider each term in detail. Let (x, y) label a dimer on the triangular lattice. The hopping part of the Hamiltonian is then

$$H_T = \sum_{\alpha} t_{\alpha} \sum_{(x,y),i} \sum'_{(x',y'),j} \sum_{\sigma} c_{(x',y'),j,\sigma}^{\dagger} c_{(x,y),i,\sigma}, \quad (2)$$

where $i = 1, 2$ labels the lattice sites on dimer (x, y) , $j = 1, 2$ labels the lattice sites on dimer (x', y') , spin is labeled by $\sigma = \uparrow, \downarrow$, and $\alpha = d, b, p, q$ specifies the type of hopping, following the notation of Ref. [28]. The restriction that (x', y') , j are limited to nearest neighbor sites and dimers is denoted by the prime on the sum. The operator $c_{(x',y'),j,\sigma}^{\dagger}$ creates an electron of spin σ on lattice site j of dimer (x', y') . Similarly, $c_{(x,y),i,\sigma}$ destroys an electron of spin σ on lattice site i of dimer (x, y) .

The onsite interaction term is given by

$$H_U = U \sum_{(x,y)} \sum_i n_{(x,y),i,\uparrow} n_{(x,y),i,\downarrow}, \quad (3)$$

with the number operator on site i of dimer (x, y) for an electron of spin σ given by $n_{(x,y),i,\sigma} = c_{(x,y),i,\sigma}^{\dagger} c_{(x,y),i,\sigma}$, and the nearest neighbor interaction Hamiltonian is

$$H_V = \sum_{\alpha} V_{\alpha} \sum_{(x,y),i} \sum'_{(x',y'),j} \sum_{\sigma,\sigma'} n_{(x',y'),j,\sigma} n_{(x,y),i,\sigma'}. \quad (4)$$

Density functional theory calculations [34–36] have predicted that the number of free electrons in κ -(BEDT-TTF)₂X salts is equal to the number of dimers. Measurements of the out-of-plane optical conductivity have also been performed for various κ -(BEDT-TTF)₂X salts, and the locations of vibrational modes were found to be consistent with one electron per dimer [12].

In the limit that U and V_d are much larger than other microscopic energy scales, these terms will strongly penalize double occupancy of dimers, and we can expect the low-energy physics to be dominated by singly occupied dimers for

$$\frac{t_{\alpha}}{U}, \frac{t_{\alpha}}{V_{\alpha}}, \frac{V_{\alpha}}{U} \ll 1. \quad (5)$$

In the low-energy limit, with single occupancy of dimers, there are four possible states per dimer, which we may write as $|\uparrow, 0\rangle$, $|\downarrow, 0\rangle$, $|0, \uparrow\rangle$, and $|0, \downarrow\rangle$, where we list the occupation of site 1 before that of site 2. We can view the dipole moment of the dimer as a pseudospin with site 1 corresponding to $P^z = \frac{1}{2}$ and site 2 corresponding to $P^z = -\frac{1}{2}$ and switch to the $|P^z, S^z\rangle$ basis to represent the state of each dimer [28].

We use a strong-coupling expansion for the extended Hubbard model, Eq. (1), to derive a low-energy effective model. We project to the one electron per dimer limit and make use of the method set out in Ref. [37]. The effective model we derive follows the approach of Hotta [28] to write the Hamiltonian in the dipole-spin basis. However, we go beyond the expansion considered by Hotta [28] by including all nearest neighbor interactions, leading to modified couplings in the low-energy effective theory.

A. Low-energy theory

In the standard strong-coupling expansion of the Hubbard model, e.g., Ref. [37], one projects onto the single electron per site limit. The situation we consider is slightly more complicated in that we consider the one electron per dimer limit. An additional complication is the presence of nearest neighbor interactions since the occupation of sites on adjacent dimers will affect the allowed terms in the expansion. To include these terms, we follow closely the approach used in Refs. [32,33] for the extended Hubbard model on a square lattice, modifying their approach for a triangular lattice of dimers.

We write the Hamiltonian in the form:

$$H = H_0 + H_T, \quad (6)$$

where $H_0 = H_U + H_V$. Here, H_0 does not change the number of electrons per dimer, whereas H_T includes hops which may

change the dimer occupation (the intradimer hopping does not change the dimer occupation, but since it can change the nearest neighbor interaction energy, we do not include it in H_0). We introduce a canonical unitary transformation S so that H_0 remains a constant of motion to a desired order in $1/U$. Let H' be the transformed Hamiltonian, then

$$H' = H_0 + H'_T, \quad (7)$$

where

$$H'_T = \exp(iS)H_T \exp(-iS), \quad (8)$$

and to ensure that H_0 remains a constant of motion to order $1/U$, we must have

$$[H_0, H'_T] = 0, \quad (9)$$

and expanding S in powers of $1/U$, we get

$$S = -i \sum_{n=1}^{\infty} \frac{S_n}{U^n}. \quad (10)$$

Since we consider the expansion to the second order in perturbation theory, we must determine both S_1 and S_2 . Expanding the hopping part of the Hamiltonian in a power series in $1/U$ also,

$$H'_T = \sum_{n=1}^{\infty} \frac{H'_{T,n}}{U^{n-1}}, \quad (11)$$

and using Eqs. (8), (10), and (11), we obtain the following expressions for the first- and second-order corrections:

$$H'_{T,1} = H_T + [S_1, \tilde{H}_0], \quad (12)$$

and

$$H'_{T,2} = [S_1, H_T] + \frac{1}{2} \{S_1, [S_1, \tilde{H}_0]\} + [S_2, \tilde{H}_0], \quad (13)$$

where $\tilde{H}_0 = H_0/U$. These equations do not give a clear path for obtaining S_1 or S_2 , but applying the equation of motion requirement Eq. (9) and demanding that it apply at each order sequentially gives

$$\{H_0, [S_1, \tilde{H}_0] + H_T\} = 0, \quad (14)$$

and

$$(H_0, \{S_1, [S_1, H_T]\} + \frac{1}{2} \{S_1, [S_1, \tilde{H}_0]\} + [S_2, \tilde{H}_0]) = 0. \quad (15)$$

To determine the solutions of Eqs. (14) and (15), it is helpful to decompose the hopping term in the Hamiltonian into channels

that are differentiated by whether they change the occupation of a dimer, like the procedure used at the site level in Ref. [37]. Define the hole occupancy $h_{(x,y),i,\sigma} = 1 - n_{(x,y),i,\sigma}$, which is 0 if site $(x, y), i$ is occupied by an electron with spin σ and 1 otherwise. Using the identity $h_{(x,y),i,\sigma} + n_{(x,y),i,\sigma} = 1$ and acting from both the right and the left, we may write $H_T = \sum_{\alpha} (T_{\alpha}^1 + T_{\alpha}^0 + T_{\alpha}^{-1})$, where (with $\bar{\sigma}$ indicating the opposite spin to σ)

$$T_{\alpha}^1 = t_{\alpha} \sum_{(x,y),i} \sum'_{(x',y'),j} \sum_{\sigma} n_{(x',y'),j,\bar{\sigma}} c_{(x',y'),j,\sigma}^{\dagger} c_{(x,y),i,\sigma} h_{(x,y),i,\bar{\sigma}}, \quad (16)$$

$$T_{\alpha}^0 = t_{\alpha} \sum_{(x,y),i} \sum'_{(x',y'),j} \sum_{\sigma} [n_{(x',y'),j,\bar{\sigma}} c_{(x',y'),j,\sigma}^{\dagger} c_{(x,y),i,\sigma} n_{(x,y),i,\bar{\sigma}} + h_{(x',y'),j,\bar{\sigma}} c_{(x',y'),j,\sigma}^{\dagger} c_{(x,y),i,\sigma} h_{(x,y),i,\bar{\sigma}}], \quad (17)$$

$$T_{\alpha}^{-1} = t_{\alpha} \sum_{(x,y),i} \sum'_{(x',y'),j} \sum_{\sigma} h_{(x',y'),j,\bar{\sigma}} c_{(x',y'),j,\sigma}^{\dagger} c_{(x,y),i,\sigma} n_{(x,y),i,\bar{\sigma}}. \quad (18)$$

Writing the summand as $(T_{\alpha}^m)_{(x,y;x',y'),i,j,\sigma}$, with $m \in \{1, 0, -1\}$, the hopping term may be written as

$$H_T = \sum_{\alpha} \sum_{(x,y),i} \sum'_{(x',y'),j} \sum_{\sigma,m} (T_{\alpha}^m)_{(x,y;x',y'),i,j,\sigma}. \quad (19)$$

Note that each T_{α}^m channel changes the number of doubly occupied sites by m , and so the interaction energy in H_0 changes by an amount mU . However, nearest neighbor interactions mean that hops that change site occupation also change nearest neighbor interaction energies. To deal with this, we follow Ref. [33] and introduce a nearest neighbor projection operator, which projects out all states except those which have an electronic configuration \tilde{n}^{β} neighboring site $(x, y), i$. Formally, it is defined as

$$O_{(x,y),i}^{\beta}[\tilde{n}^{\beta}] = \prod_{(\delta_{\beta x}, \delta_{\beta y}, \delta_{\beta})_{\sigma}} \{ \tilde{n}_{(\delta_{\beta x}, \delta_{\beta y}, \delta_{\beta})_{\sigma}} n_{(x+\delta_{\beta x}, y+\delta_{\beta y}), i+\delta_{\beta}, \sigma} + [1 - \tilde{n}_{(\delta_{\beta x}, \delta_{\beta y}, \delta_{\beta})_{\sigma}}] h_{(x+\delta_{\beta x}, y+\delta_{\beta y}), i+\delta_{\beta}, \sigma} \}, \quad (20)$$

where the $(\delta_{\beta x}, \delta_{\beta y}, \delta_{\beta})$ connecting site $(x, y), i$ to the neighboring sites via $\beta = d, b, p, q$ and $\tilde{n}_{(\delta_{\beta x}, \delta_{\beta y}, \delta_{\beta})_{\sigma}}$ is 1 when the site at $(x + \delta_{\beta x}, y + \delta_{\beta y}), i + \delta_{\beta}$ is occupied and zero otherwise. Inserting forms of the identity:

$$1 = \prod_{(\delta_{\beta x}, \delta_{\beta y}, \delta_{\beta})_{\sigma}} [n_{(x+\delta_{\beta x}, y+\delta_{\beta y}), i+\delta_{\beta}, \sigma} + h_{(x+\delta_{\beta x}, y+\delta_{\beta y}), i+\delta_{\beta}, \sigma}],$$

on either side of Eq. (19), one can find (like Ref. [33])

$$H_T = \sum_{\alpha, m, \{M_1\}, \{M_2\}} T_{\alpha}^{m, \{M_2\}, \{M_1\}}, \quad (21)$$

where $\{M_1\} = \{M_1^d, M_1^b, M_1^p, M_1^q\}$ indicates the number of occupied neighboring d , b , p , and q sites before the hop, and $\{M_2\}$ indicates the neighbors after the hop. Hence,

$$T_\alpha^{m, \{M_2\}, \{M_1\}} = t_\alpha \sum_{(x,y),i} \sum'_{(x',y'),j} \sum_\sigma \left\{ \prod_\beta \sum_{S[n_2^\beta]=M_2^\beta} \sum_{S[n_1^\beta]=M_1^\beta} \right\} \\ \times \left\{ \prod_\gamma O_{(x',y'),j}^\gamma [n_2^\gamma] \right\} (T_\alpha^m)_{(x,y),i,j,\sigma} \\ \times \left\{ \prod_\eta O_{(x,y),i}^\eta [n_1^\eta] \right\}, \quad (22)$$

and $S[n^\beta] = \sum_{(\delta_{\beta x}, \delta_{\beta y}, \delta_\beta), \sigma} n_{(\delta_{\beta x}, \delta_{\beta y}, \delta_\beta), \sigma}$ is the total number of occupied neighboring sites of type β . The different hopping channel operators have the commutators (see Appendix C for a derivation):

$$[H_U + H_V, T_\alpha^{m, \{M_2\}, \{M_1\}}] = \left[mU + \sum_\beta V_\beta (M_2^\beta - M_1^\beta) \right] \\ \times T_\alpha^{m, \{M_2\}, \{M_1\}}, \quad (23)$$

and using the decomposition in Eq. (21) with the commutator Eq. (23) allows one to obtain S_1 and S_2 , as outlined in Appendix B. The first-order correction is

$$H'_{T,1} = \sum_\alpha \sum_{\{M\}} T_\alpha^{0, \{M\}, \{M\}}, \quad (24)$$

and the second-order correction is

$$H'_{T,2} = U \sum_{\alpha, \nu} \sum_{\tilde{\{M_2\}, \{M_1\}, \{N\}, m}} \\ \times \frac{T_\alpha^{m, \{M_2\}, \{M_1\}} T_\nu^{-m, \{N\}, \{M_2\} - \{M_1\} + \{N\}}}{mU + \sum_\gamma V_\gamma (M_2^\gamma - M_1^\gamma)}, \quad (25)$$

where the tilde on the sum over occupation numbers indicates that the sum excludes values of m , $\{M_1\}$ and $\{M_2\}$ for which the denominator vanishes.

The first-order correction corresponds to a process with a single hop, which can only maintain the one electron per dimer limit if it is an intradimer hop, i.e., $\alpha = d$; no other hops are allowed. It also requires that the number of nearest neighbor electrons is the same before and after the hop. In summary, the full second-order effective Hamiltonian is

$$H' = H_U + H_V + \sum_{\{M\}} T_d^{0, \{M\}, \{M\}} + \sum_{\alpha, \nu} \sum_{\tilde{\{M_2\}, \{M_1\}, \{N\}, m}} \\ \times \frac{T_\alpha^{m, \{M_2\}, \{M_1\}} T_\nu^{-m, \{N\}, \{M_2\} - \{M_1\} + \{N\}}}{mU + \sum_\gamma V_\gamma (M_2^\gamma - M_1^\gamma)}. \quad (26)$$

We now proceed to write the low-energy model in terms of dipole and spin operators, following Hotta [28]. The full form of the effective low-energy model in the dipole-spin basis is

$$H' = V_q \sum_i \sum_j' P_i^z P_j^z - V_p \sum_i \sum_j' P_i^z P_j^z - V_b \sum_i \sum_j' P_i^z P_j^z + t_d \sum_i (P_i^+ + P_i^-) \\ + \sum_i \sum_j' [C_{i,j}^0 P_i^z P_j^z + C_{i,j}^1 P_i^z P_j^z + C_{i,j}^2 P_i^z P_j^z + C_{i,j}^3 \vec{S}_i \cdot \vec{S}_j + C_{i,j}^4 P_i^z \vec{S}_i \cdot \vec{S}_j + C_{i,j}^5 P_j^z \vec{S}_i \cdot \vec{S}_j \\ + C_{i,j}^6 P_i^z P_j^z \vec{S}_i \cdot \vec{S}_j + C_{i,j}^7 (P_i^+ + P_i^-) + C_{i,j}^8 (P_i^+ P_j^z + P_i^- P_j^z) + C_{i,j}^9 (P_i^+ \vec{S}_i \cdot \vec{S}_j + P_i^- \vec{S}_i \cdot \vec{S}_j) \\ + C_{i,j}^{10} (P_i^+ P_j^z \vec{S}_i \cdot \vec{S}_j + P_i^- P_j^z \vec{S}_i \cdot \vec{S}_j) + C_{i,j}^{11} (P_j^+ + P_j^-) + C_{i,j}^{12} (P_j^+ P_i^z + P_j^- P_i^z) \\ + C_{i,j}^{13} (P_j^+ \vec{S}_i \cdot \vec{S}_j + P_j^- \vec{S}_i \cdot \vec{S}_j) + C_{i,j}^{14} (P_j^+ P_i^z \vec{S}_i \cdot \vec{S}_j + P_j^- P_i^z \vec{S}_i \cdot \vec{S}_j)], \quad (27)$$

where the various $C_{i,j}^n$ are listed in Appendix C 1. When viewed as a spin model for the dipole pseudospins, the model has ferromagnetic interactions (V_p and V_b), antiferromagnetic interactions (V_q), and interactions between dipoles that depend on the states of the physical spins of the dimers (the $C_{i,j}^n$). There are also random-field like terms for the dipoles that depend on the occupations of nearest neighbors. Given that the model sits on a triangular lattice, this suggests that there may be frustrating interactions between the dipoles that could possibly lead to slow dynamics and/or glassy behavior. Performing a dynamical simulation of this model for more than a small number of spins and dipoles is not practical due to the quantum terms involving dipole raising and lowering operators P^+ and P^- .

Hence, in an effort to learn whether this low-energy model contains glassy physics, we drop the quantum terms and focus on a simplified classical spin model of dipoles coupled to

spins on a triangular lattice:

$$H_{\text{classical}} = V_q \sum_i \sum_j' P_i^z P_j^z - V_p \sum_i \sum_j' P_i^z P_j^z \\ - V_b \sum_i \sum_j' P_i^z P_j^z + \sum_i \sum_j' (C_{i,j}^0 P_i^z + C_{i,j}^1 P_j^z \\ + C_{i,j}^2 P_i^z P_j^z + C_{i,j}^3 \vec{S}_i \cdot \vec{S}_j + C_{i,j}^4 P_i^z \vec{S}_i \cdot \vec{S}_j + C_{i,j}^5 \\ \times P_j^z \vec{S}_i \cdot \vec{S}_j + C_{i,j}^6 P_i^z P_j^z \vec{S}_i \cdot \vec{S}_j). \quad (28)$$

We treat the dipoles P_i^z as Ising variables and the spins \mathbf{S}_i as classical vectors. While this approximation is uncontrolled, it does allow the model to be simulated using classical Monte Carlo techniques.

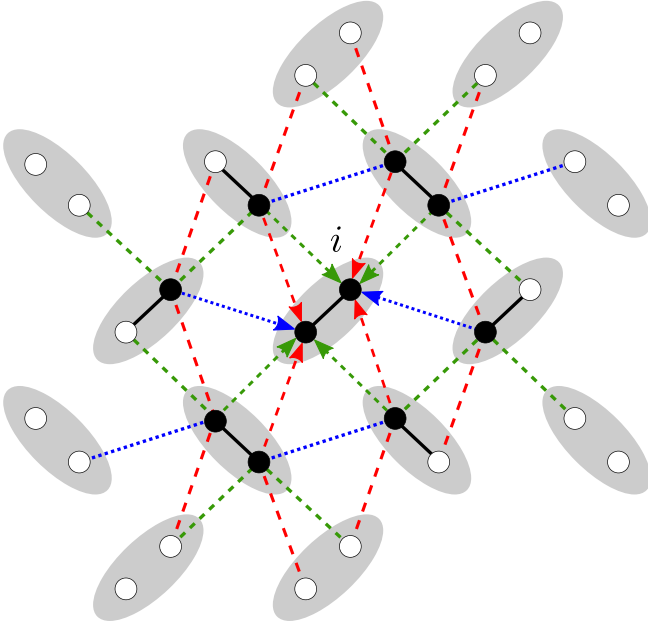


FIG. 2. Dimers that must be included to calculate couplings for the dimer i . Each black dot represents a lattice site for which the nearest neighbor occupancy needs to be known to properly calculate each C_n , meaning that a minimum of 15 dimers are needed to calculate the full set of couplings.

III. MONTE CARLO SIMULATIONS

In this section, we present and discuss results from equilibrium Monte Carlo simulations of the model defined in Eq. (28). We calculate the polarization, magnetization, electric and magnetic susceptibility, and Edwards-Anderson order parameters for both spin and charge degrees of freedom. The couplings in $H_{\text{classical}}$ depend not only on the parameters of the extended Hubbard model but also on the occupation of the neighboring sites in the lattice. This means that the couplings in a Monte Carlo simulation depend on the state of the system and will evolve as dipoles are flipped. To obtain a more computationally tractable problem, we instead use the following procedure to specify the model: (i) calculate the distribution of all possible values of couplings for each term in the Hamiltonian, (ii) fit the distribution to a simplified form, (iii) draw couplings between dipoles and spins randomly from the distributions calculated in (ii), and (iv) average over multiple sets of couplings.

Each of the coefficients C_{ij}^n in Eq. (28) is determined by the electronic configurations of the neighboring dimers (see Tables I–IV in Appendix C). Therefore, for each distinct electronic configuration of nearest neighbors about some central dimer i , there will be a different set of $C_{i,j}^n$ for that dimer. For large lattices, calculating the couplings for each dimer is a very computationally expensive task. To run Monte Carlo simulations, one must first calculate the set of couplings $C_{i,j}^n$ from the set of C_n , as set out in Appendix C. To simplify the calculations, we find the distributions of the various $C_{i,j}^n$ and then sample from these distributions to set the couplings for each simulation. In this way, we aim to capture the effect of

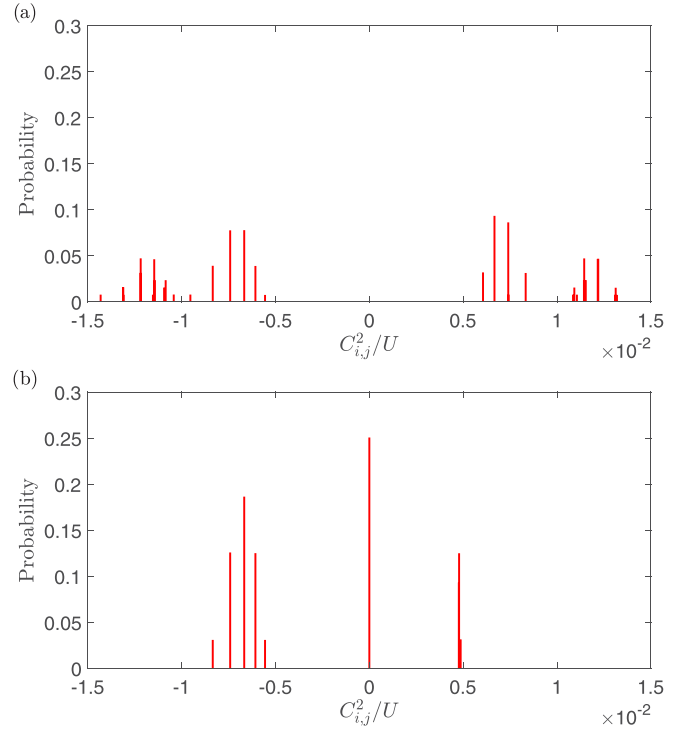


FIG. 3. Normalized probability distributions for $C_{i,j}^2$ couplings to the two types of dimers neighboring a central dimer located at $i = (x, y)$. (a) $(x \pm \frac{1}{2}, y \pm \frac{1}{2})$ neighbors; (b) $(x \pm 1, y)$ neighbors. Each bar has a width of 1.4×10^{-5} . Parameters used are $U/t = 15.000113$, $V_d/t = 10.000219$, $V_b/t = 1.000547$, $V_p/t = 1.000623$, and $V_q/t = 1.000412$.

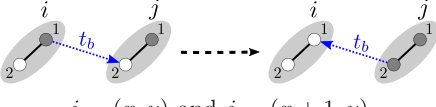

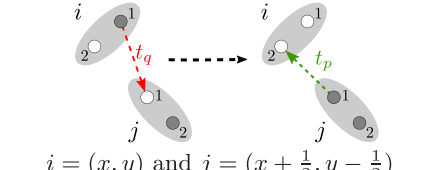
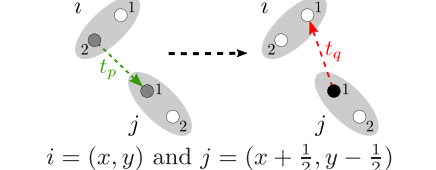
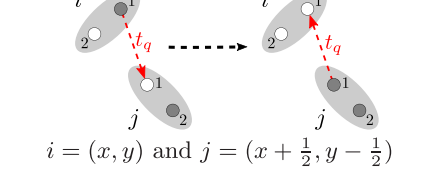
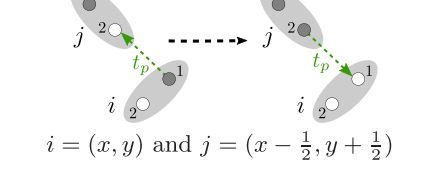
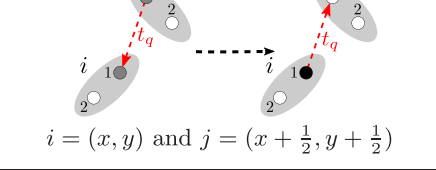
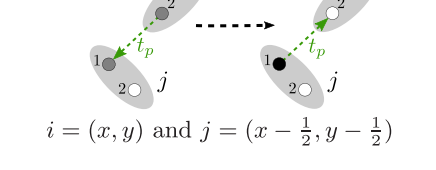
the distribution of couplings that arise from the different occupations without recalculating all of the couplings at each step of the calculation as dipoles flip and the charge distribution evolves with time.

We now discuss the calculation of the couplings. The denominator of each C_n relating to the hopping between dimers i and j depends on the occupancy of the nearest neighbors of a lattice site on dimer j as well as the occupancy of the nearest neighbors of a lattice site on the dimer i . As can be seen in Fig. 2, this implies that, to calculate a set of C_n , the electronic configuration of a dimer i as well as its 14 nearest and next-nearest neighbors must be known.

We calculated the distributions of the $C_{i,j}^n$ as follows: first, for a single 15 dimer electronic configuration, we calculated the set of C_n . Second, we used the set of C_n to calculate the corresponding set of $C_{i,j}^n$ (Appendix C 1). We repeated this process until the electronic configuration space was properly sampled and binned the various $C_{i,j}^n$ to create histograms. There are $2^{15} = 32\,768$ possible electronic configurations.

While motivated by the κ -(BEDT-TTF) $_2X$ family of salts, we do not choose parameter values for any specific material but are somewhat guided by the parameter choices in Ref. [28]. In all calculations, we take the hopping parameters to be $t_b = t_p = t_q = t$, and measuring other parameters in terms of t , we take $U = 15t$, with V_d taking values between $4t$ and $12t$ and V_b, V_p , and V_q taking values between t and

TABLE I. Examples of second-order processes for each of the couplings C_1 to C_8 .

Process	Contribution to Hamiltonian
 $i = (x, y)$ and $j = (x + 1, y)$	$C_1(\frac{1}{2} + P_i^z)(\frac{1}{2} + P_j^z)$
 $i = (x, y)$ and $j = (x + 1, y)$	$C_2(\frac{1}{2} + P_i^z)(\frac{1}{2} - P_j^z)(\frac{1}{2} - 2\vec{S}_i \cdot \vec{S}_j)$
 $i = (x, y)$ and $j = (x + \frac{1}{2}, y - \frac{1}{2})$	$C_3(\frac{1}{2} - P_j^z)P_i^-$
 $i = (x, y)$ and $j = (x + \frac{1}{2}, y - \frac{1}{2})$	$C_4(\frac{1}{2} + P_j^z)P_i^-(\frac{1}{2} - 2\vec{S}_i \cdot \vec{S}_j)$
 $i = (x, y)$ and $j = (x + \frac{1}{2}, y - \frac{1}{2})$	$C_5(\frac{1}{2} + P_i^z)(\frac{1}{2} - P_j^z)$
 $i = (x, y)$ and $j = (x - \frac{1}{2}, y + \frac{1}{2})$	$C_6(\frac{1}{2} + P_i^z)(\frac{1}{2} + P_j^z)$
 $i = (x, y)$ and $j = (x + \frac{1}{2}, y + \frac{1}{2})$	$C_7(\frac{1}{2} + P_i^z)(\frac{1}{2} + P_j^z)(\frac{1}{2} - 2\vec{S}_i \cdot \vec{S}_j)$
 $i = (x, y)$ and $j = (x - \frac{1}{2}, y - \frac{1}{2})$	$C_8(\frac{1}{2} - P_i^z)(\frac{1}{2} + P_j^z)(\frac{1}{2} - 2\vec{S}_i \cdot \vec{S}_j)$

$3t$. For reference, Pinterić *et al.* [13] estimate $U/t = 7.3$ in κ -(BEDT-TTF) $_2$ Cu $_2$ (CN) $_3$. The choice of all hopping parameters being equal leads to some coupling coefficients being equal that would otherwise take on different values.

There is a subtlety involved when calculating the denominators of the set of C_n . As discussed in Appendix C, the strong-coupling expansion excludes all terms which have a zero denominator. The denominator takes the form

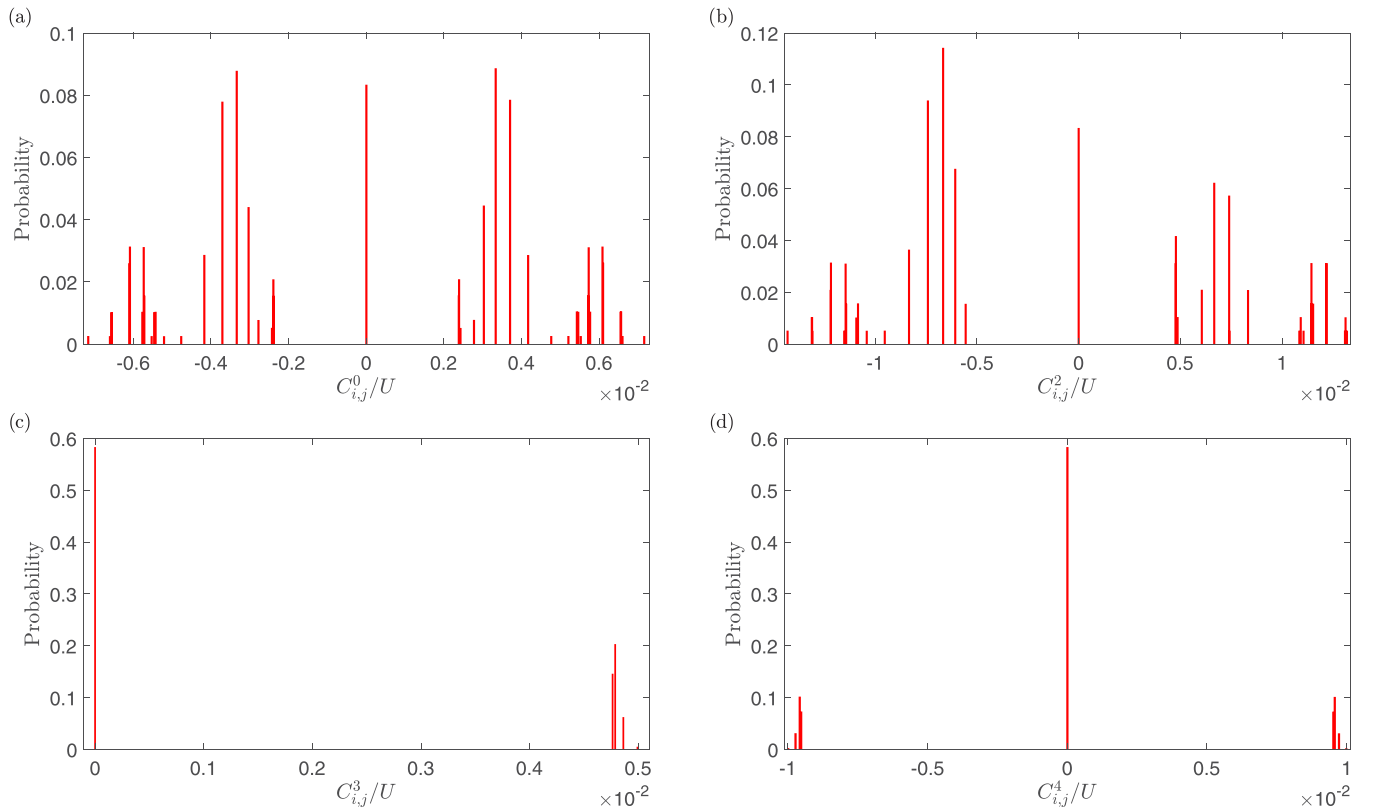


FIG. 4. Histograms combining couplings for all neighboring dimers for various C_{ij}^n couplings: (a) C_{ij}^0 , (b) C_{ij}^2 , (c) C_{ij}^3 , and (d) C_{ij}^4 . Parameters used are the same as Fig. 3.

$mU + \sum_{\gamma} V_{\gamma}(M_2^{\gamma} - M_1^{\gamma})$, where m and $(M_2^{\gamma} - M_1^{\gamma})$ are integers, implying that, if the U and the V_{γ} are factors of each other, it is possible to have a vanishing denominator. According to the strong-coupling expansion, if a process leads to a vanishing denominator, it does not contribute to the second-order Hamiltonian. To avoid such terms, we selected parameters U and V_{γ} such that the denominator does not vanish.

We determined histograms for all couplings C_{ij}^n that enter into the effective model. Examples of these histograms for C_{ij}^1 (which give the strengths of the $P_i^z P_j^z$ interaction) are

shown in Fig. 3. The couplings to dimers $(x \pm \frac{1}{2}, y \pm \frac{1}{2})$ are identical due to symmetry for the chosen hopping parameters as are those to dimers located at $(x \pm 1, y)$, so there are only two types of C_{ij}^1 couplings for our choice of parameters. The combined distributions of all C_{ij}^0 , C_{ij}^2 , C_{ij}^3 , and C_{ij}^4 couplings are shown in Fig. 4.

As a further simplification, we find approximate analytical forms for the distributions and draw the couplings from these approximate distributions. Many parameter choices lead to histograms which can be modeled adequately by a probability density function of the form:

$$P(x) = \begin{cases} 0, & x < w_1, \\ b_1, & w_1 \leq x < w_2, \\ 0, & w_2 \leq x < 0, \\ [1 - b_2(w_4 - w_3) - b_1(w_2 - w_1)]\delta(x), & x = 0, \\ 0, & 0 < x \leq w_3, \\ b_2, & w_3 < x \leq w_4, \\ 0, & w_4 < x, \end{cases} \quad (29)$$

with $w_4 > w_3 > w_2 > w_1$ and $b_1 \geq 0$, $b_2 \geq 0$. A general graphical representation of this distribution is shown in Fig. 5 using C_{ij}^0 as an example.

We select the w_n and b_n parameters so that the corresponding cumulative probability function obtained from Eq. (29) matches the cumulative probability function of the various histograms. This ensures that the behavior of the distribution

is properly captured. We first choose the parameters w_n based on the cumulative probability function of the various histograms and then perform a least squares analysis to calculate the b_n fitting parameters. This process ensures that all the desired peaks are captured and is performed for every fit. Some results of this fitting procedure are shown in Fig. 6 for C_{ij}^0 and C_{ij}^4 .

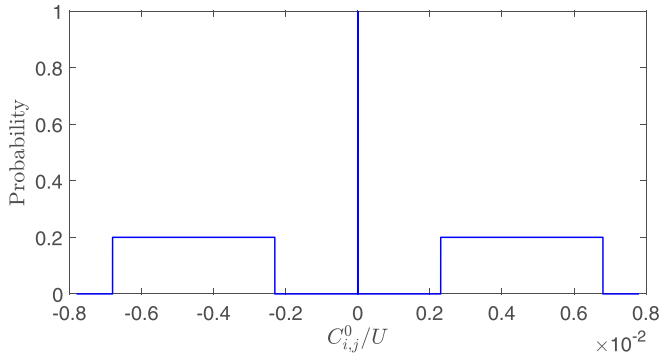


FIG. 5. An example of the approximate probability density function shown in Eq. (29) for C_{ij}^0 : here, $w_1 = -0.0068$, $w_2 = -0.0023$, $w_3 = 0.0023$, $w_4 = 0.0068$, and $b_1 = b_2 = 0.2$.

In the Monte Carlo simulations, we create a triangular lattice of N dimers and then assign couplings randomly from the calculated distributions. As there are many more coupling configurations than N , we average over couplings to obtain a representative sample of the configuration space. In one Monte Carlo step, we attempt to flip N spins and N dipoles, choosing spins and dipoles at random. A spin flip corresponds to assigning a new direction in space for the vector spin and flipping a dipole corresponds to changing the sign of the Ising degree of freedom. We use the METROPOLIS algorithm to determine the probability of whether a move that leads to an energy change ΔE is accepted:

$$P(\Delta E) = \begin{cases} 1, & \Delta E \leq 0, \\ \exp(-\beta \Delta E), & \Delta E > 0, \end{cases} \quad (30)$$

where $\beta = 1/(k_B T)$ with $k_B = 1.38 \times 10^{-23} \text{ m}^2 \text{ J K}^{-1}$.

We consider lattices of up to $N = 14^2 = 196$ dimers and establish equilibration by considering two replicas of the system, prepared with the same set of couplings but different thermal histories (i.e., different random numbers in the METROPOLIS algorithm). One replica is initialized with completely polarized spins and dipoles and the other with

completely random spins and dipoles. We then evolve the system, and it is taken to be equilibrated when chosen thermodynamic variables (the electric and magnetic susceptibilities) calculated in the two replicas agree to within a tolerance of 2%. After the system has equilibrated, we sample to obtain averages of the quantities that we discuss below.

First, we calculate the average polarization per dipole at time step t_j for a lattice size of N dimers, given by

$$P(t_j) = \frac{1}{N} \left| \sum_{i=1}^N P_i(t_j) \right|, \quad (31)$$

with $P_i(t_j)$ the polarization of dimer i at time step t_j . Second, we calculate the average magnetization per spin at time step t_j :

$$M(t_j) = \frac{1}{N} \left| \sum_{i=1}^N \vec{S}_i(t_j) \right|, \quad (32)$$

where $\vec{S}_i(t_j)$ is the spin of dimer i at time step t_j . We then calculate the average polarization $P = \langle P(t_j) \rangle$ and average magnetization $M = \langle M(t_j) \rangle$, where the notation $\langle \dots \rangle$ indicates a time average over N_t Monte Carlo time steps. We also calculate the electric susceptibility and magnetic susceptibility, defined respectively as

$$\chi_P = \beta \lim_{t_j \rightarrow \infty} (\langle P(t_j)^2 \rangle - \langle P(t_j) \rangle^2), \quad (33)$$

and

$$\chi_M = \beta \lim_{t_j \rightarrow \infty} (\langle M(t_j)^2 \rangle - \langle M(t_j) \rangle^2). \quad (34)$$

Our equilibration criterion is that the electric and magnetic susceptibilities of the two replicas agree to 2% tolerance or completion of 2×10^7 Monte Carlo time steps, whichever comes first. We were unable to reach equilibrium at temperatures $< 0.0065 U/k_B$.

To check for glassy behavior we calculate the Edwards-Anderson order parameters for both charge and spin degrees of freedom. For the Ising-like dipole degrees of freedom, the Edwards-Anderson order parameter is

$$Q_{\text{EA}}^{\text{Pol}} = \lim_{t_j \rightarrow \infty} \left[\overline{\left\langle \left\langle \frac{1}{N} \sum_{i=1}^N P_i^{z,A}(t_j) P_i^{z,B}(t_j) \right\rangle - \left\langle \sum_{i=1}^N P_i^{z,A}(t_j) \right\rangle \left\langle \sum_{i=1}^N P_i^{z,B}(t_j) \right\rangle \right\rangle} \right]. \quad (35)$$

Here, $P_i^{z,A}(t_j)$ and $P_i^{z,B}(t_j)$ are the z components of polarization on dimer i at time step t_j for replicas A and B , respectively. The overbar indicates an average over the bond configurations. For a lattice of N dimers, the Edwards-Anderson order parameter for the spin degrees of freedom takes the form:

$$Q_{\text{EA}}^{\text{Mag}} = \lim_{t_j \rightarrow \infty} \left[\overline{\left\langle \left\langle \frac{1}{N} \sum_{i=1}^N \vec{S}_i^A(t_j) \cdot \vec{S}_i^B(t_j) \right\rangle - \left\langle \sum_{i=1}^N \vec{S}_i^A(t_j) \right\rangle \cdot \left\langle \sum_{i=1}^N \vec{S}_i^B(t_j) \right\rangle \right\rangle} \right], \quad (36)$$

where $\vec{S}_i^A(t_j)$ and $\vec{S}_i^B(t_j)$ are the spins at dimer i at time step t_j for replicas A and B , respectively.

To establish whether there is a phase transition and, if so, to estimate of the critical temperature T_c , we use the Binder cumulant statistic. For the Edwards-Anderson order parameter

Q , the statistic is given by

$$U_L(Q) = \frac{3}{2} \left[1 - \frac{\langle Q^4 \rangle_L}{3 \langle Q^2 \rangle_L^2} \right], \quad (37)$$

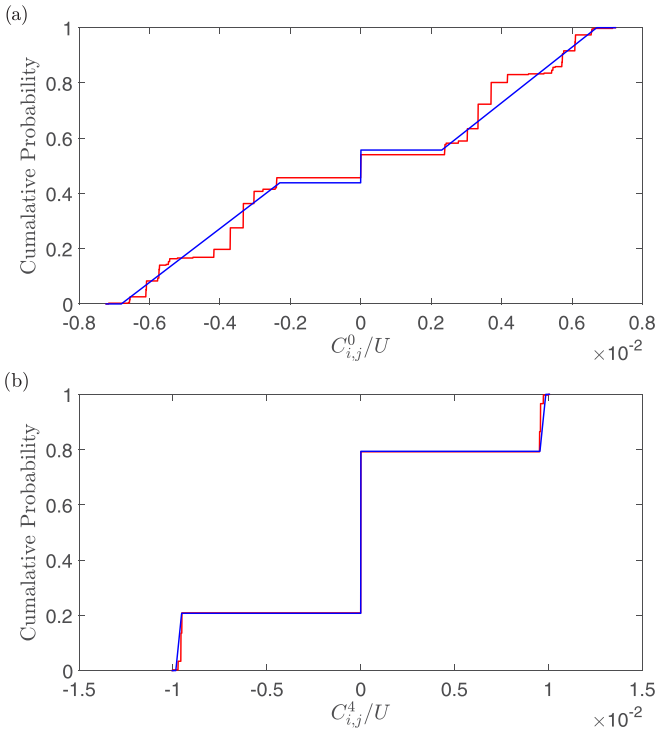


FIG. 6. Cumulative probability functions for the combined histograms of (a) $C_{i,j}^0$ and (b) $C_{i,j}^4$. The parameters used are $U/t = 15.0113$, $V_d/t = 8.0219$, $V_b/t = 1.0547$, $V_p/t = 1.0623$, and $V_q/t = 1.0412$.

where L is the size of the system. We plot U_L as a function of temperature for different system sizes. If there is a transition to an ordered phase at a temperature T_c , then in the large L limit, U_L tends to a finite value for $T < T_c$ and 0 for $T > T_c$. Up to small finite-sized corrections, the Binder cumulant curves should intersect at the critical temperature, where in the $L \rightarrow \infty$ limit, the Binder cumulant is independent of system size.

Figure 7 shows the polarization as a function of temperature for various intradimer and interdimer interaction energies, respectively. There is no evidence for ordering in the charge

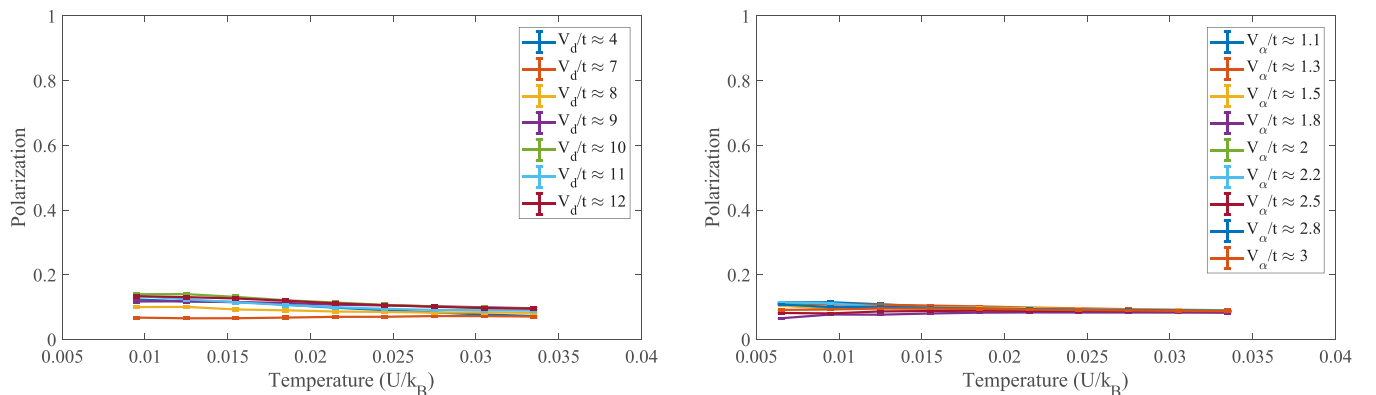


FIG. 7. Polarization averaged over 18 bond configurations as a function of temperature for a lattice size of $10^2 = 100$. (a) Fixed interdimer interactions: $U/t = 15.0113$, $V_b/t = 1.0547$, $V_p/t = 1.0623$, and $V_q/t = 1.0412$ for varying V_d/t . (b) Fixed intradimer coupling: $U/t = 15.0113$, and $V_d/t = 10.0219$ for varying V_α/t , with $\alpha = b, p, \text{ and } q$.

degrees of freedom for the parameters considered. We also see no ordering in the spin degrees of freedom shown in Fig. 8.

Figures 9 and 10 show the electric and magnetic susceptibilities as a function of temperature, respectively. We see similar behavior for a wide range of V_d and V_α for different lattice sizes of N dimers.

In Fig. 11, we show Q_{EA}^{Pol} and Q_{EA}^{Mag} as a function of temperature. In the low-temperature regime ($\lesssim 0.02 U/k_B$), Q_{EA}^{Pol} grows with decreasing temperature for $V_d/t \approx 10, 11$, and 12. For intradimer interaction energies $V_d/t \lesssim 10$, Q_{EA}^{Pol} becomes appreciable for temperatures $\lesssim 0.03 U/k_B$. Smaller intradimer interactions ($V_d/t \lesssim 10$) show stronger evidence of a nonzero Edwards-Anderson order parameter in the charge degrees of freedom at the chosen temperatures. Even though we see evidence of glassy ordering in charge degrees of freedom at low temperatures in Fig. 11, we do not see any evidence of glassy ordering in the spin degrees of freedom. Here, Q_{EA}^{Mag} takes on values indistinguishable from zero for all temperatures and V_d/t values considered.

Similar results to those seen in Fig. 11 are shown in Fig. 12, where we plot Q_{EA}^{Pol} and Q_{EA}^{Mag} as a function of temperature for different interdimer interaction energies. Here, we observe that small V_α/t values lead to a larger Q_{EA}^{Pol} at low temperatures than large V_α/t . We note that, while there is some sample-to-sample variation for different bond configurations, this is largest at the lowest temperatures.

A simple estimate of the phase transition is provided by the temperature at which the Edwards-Anderson order parameter becomes clearly distinct from zero, which can be determined from Figs. 11 and 12 to be $k_B T \approx 0.025 U/k_B$. In the following discussion, we present a quantitative estimate of the phase transition in our model obtained from the Binder cumulant statistic.

Taking $V_d/t \approx 10$, the intersection of the curves in Fig. 13 determines an estimate for the critical temperature for the phase transition of $\approx 0.022 U/k_B$ as compared with the naive estimate of $\approx 0.025 U/k_B$ obtained from the Q_{EA}^{Pol} curve in Fig. 11. We observed similar behavior for other parameter values (e.g., $V_d/t = 8$ and 9), but this is the clearest example of a transition.

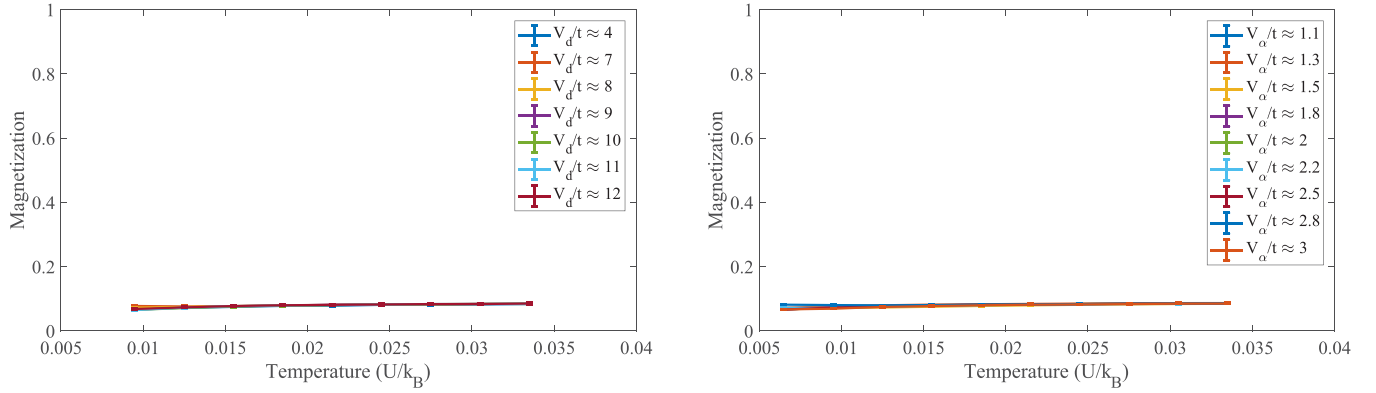


FIG. 8. Magnetization averaged over 18 bond configurations as a function of temperature for a lattice size of $10^2 = 100$. (a) Fixed interdimer interactions: $U/t = 15.0113$, $V_b/t = 1.0547$, $V_p/t = 1.0623$, and $V_q/t = 1.0412$ for varying V_d/t . (b) Fixed intradimer coupling: $U/t = 15.0113$, and $V_d/t = 10.0219$ for varying V_α/t , with $\alpha = b, p$, and q .

IV. DISCUSSION AND CONCLUSIONS

In this paper, we have considered an extended Hubbard model of dimers on a triangular lattice and obtained the low-energy effective theory in terms of separate spin and charge degrees of freedom in the one electron per dimer limit, considering the occupation of nearest neighbor sites, which extends a previous perturbative expansion of the model [28]. To study the tendency toward glassiness of charge degrees of freedom in the model, motivated by evidence of relaxor ferroelectric behavior in the κ -(BEDT-TTF) $_2X$ family of salts, we made a classical approximation to the effective model so that we could study it with Monte Carlo simulations. The couplings in the effective model depend on the occupations of the neighboring sites. Thus, to avoid recalculating the couplings at each step of the Monte Carlo simulation, we calculated the full distribution of couplings and then drew couplings randomly from this distribution. Under these conditions, we have shown that a nonzero Edwards-Anderson order parameter for charge degrees of freedom develops below a critical temperature T_c .

To make some connection to experiment, we take $U \sim 0.7$ eV [36], which would place $T_c = 0.022 U/k_B \sim 180$ K, which is much higher than the temperatures at which glassy dynamics is seen in κ -(BEDT-TTF) $_2X$ salts, which is

usually on the order of tens of kelvins. However, several of the approximations we have made are likely to enhance ordering, so it is not surprising that our temperature estimate is considerably higher than experimental observations. There are two main approximations we have made that likely enhance glassiness in the model. Both of these approximations are uncontrolled, but they are necessary to make computational progress. First, we drop quantum terms in Eq. (27), specifically P^+ and P^- , to obtain our effective model, which corresponds to ignoring quantum fluctuations. These fluctuations, which in a fully quantum problem provide dynamics to the dipoles, would otherwise be expected to depress T_c , as has been noted for transverse field Ising spin glasses [38]. Second, we draw the couplings we use in the Monte Carlo simulation from a fixed distribution that is independent of time rather than working with couplings that fluctuate with time. This has the effect of generating quenched rather than time-dependent disorder, which will also enhance glassy tendencies in the model. However, as has been shown theoretically, quenched disorder is not essential for glassy behavior [39,40]. Despite the two approximations identified above, glassiness appears quite readily in the charge degrees of freedom in the classical Monte Carlo simulations we perform. Hence, we expect that, even if the two approximations we

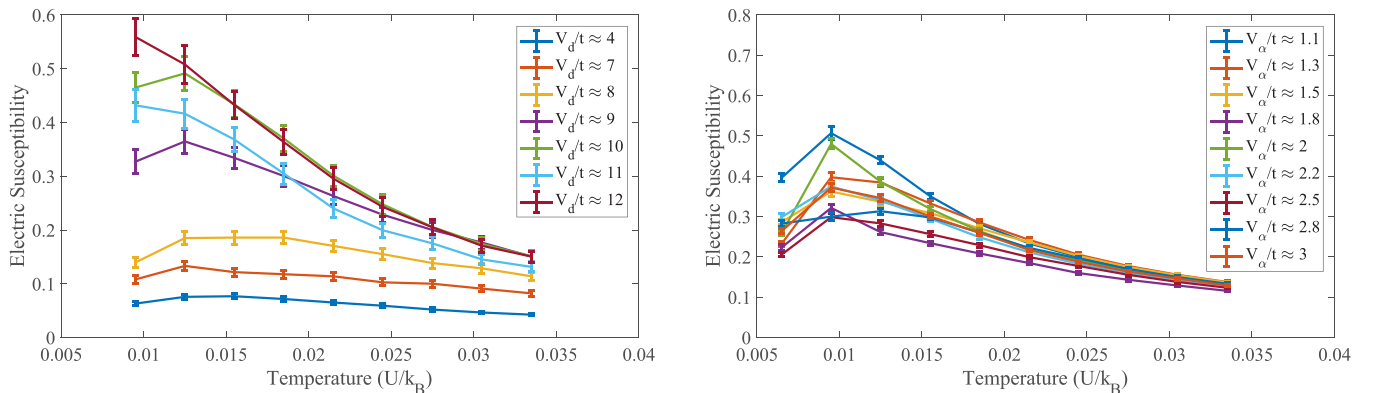


FIG. 9. Electric susceptibility averaged over 18 bond configurations as a function of temperature for a lattice size of $10^2 = 100$. (a) Fixed interdimer interactions: $U/t = 15.0113$, $V_b/t = 1.0547$, $V_p/t = 1.0623$, and $V_q/t = 1.0412$ for varying V_d/t . (b) Fixed intradimer coupling: $U/t = 15.0113$ and $V_d/t = 10.0219$ for varying V_α/t , with $\alpha = b, p$, and q .

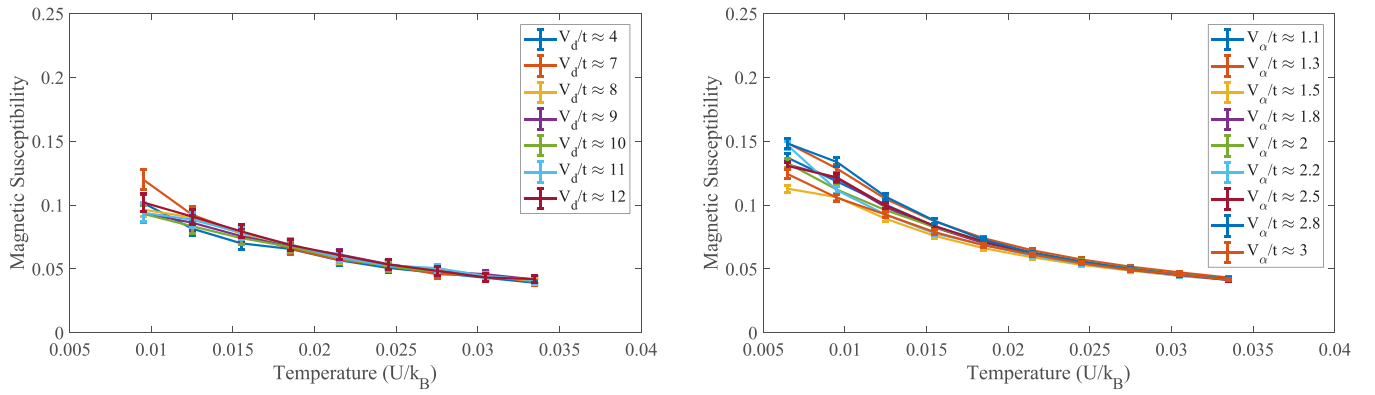


FIG. 10. Magnetic susceptibility averaged over 18 bond configurations as a function of temperature for a lattice size of $10^2 = 100$. (a) Fixed interdimer interactions: $U/t = 15.0113$, $V_b/t = 1.0547$, $V_p/t = 1.0623$, and $V_q/t = 1.0412$ for varying V_d/t . (b) Fixed intradimer coupling: $U/t = 15.0113$ and $V_d/t = 10.0219$ for varying V_α/t , with $\alpha = b, p$, and q .

have made are relaxed, it is likely that there will remain strong tendencies toward glassiness. These tendencies may manifest themselves through a reduced T_c (in some regions of parameter space, it may well be that T_c is reduced to zero) or slow dynamics, which can occur even in the absence of a glass transition [41]. Previous work on classical models of spins coupled to charge degrees of freedom has also demonstrated glassy dynamics, even in the absence of disorder [40].

Another observation of note is that we find no ordering in the spin degrees of freedom and no development of charge polarization at the temperatures we can access, consistent with the experimental observations in κ -(BEDT-TTF) $_2$ X salts. In addition, the observation of a nonzero Edwards-Anderson transition temperature in a two-dimensional model might be surprising until one considers that it is on a triangular lattice, for which each site has six neighbors, unlike the two-dimensional Edwards-Anderson model on a square lattice

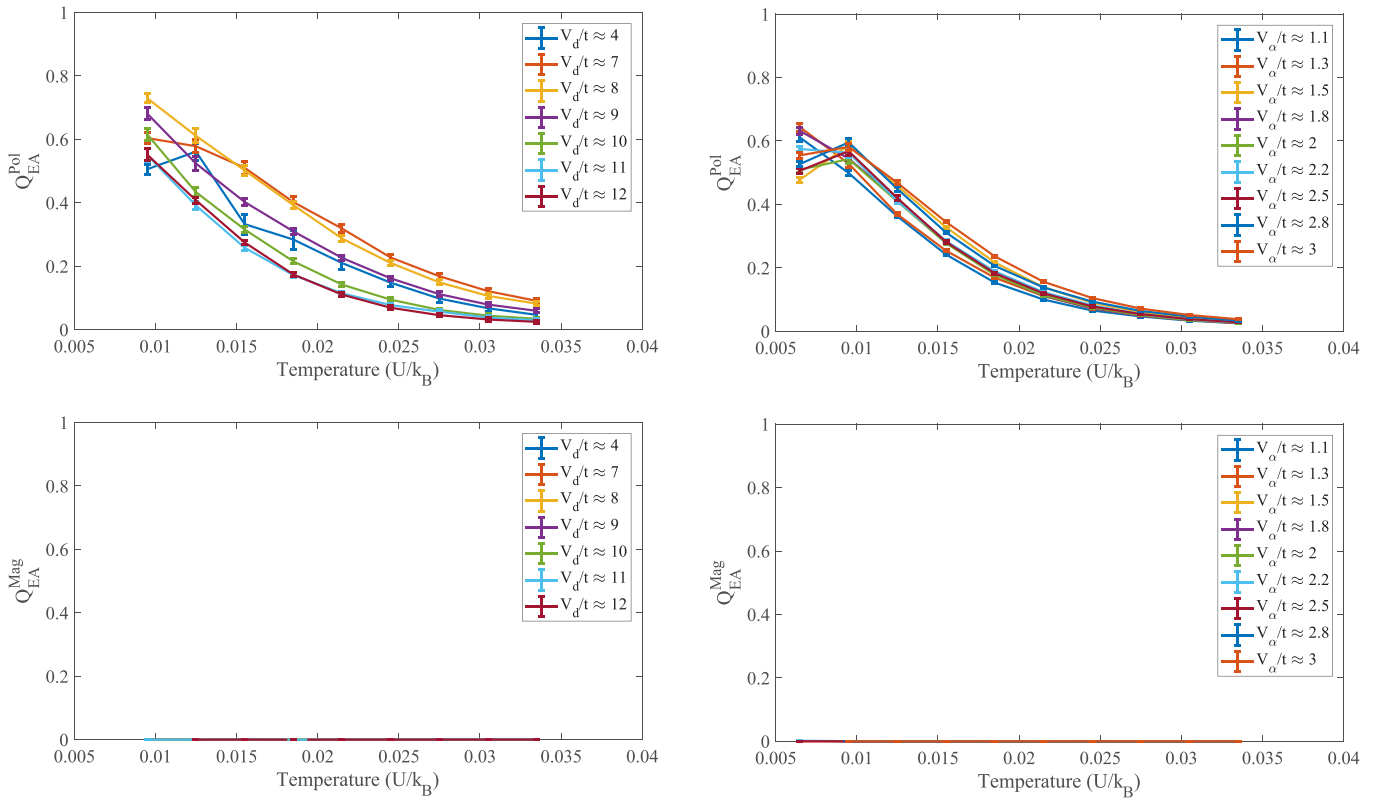


FIG. 11. (a) Q_{EA}^{Pol} and (b) Q_{EA}^{Mag} for fixed interdimer interaction strengths on a lattice of $10^2 = 100$ dimers, averaged over 18 bond configurations. The parameters used were $U/t = 15.0113$, $V_b/t = 1.0547$, $V_p/t = 1.0623$, and $V_q/t = 1.0412$ for varying V_d/t .

FIG. 12. (a) Q_{EA}^{Pol} and (b) Q_{EA}^{Mag} for fixed intradimer interaction strengths on a lattice of $10^2 = 100$ dimers, averaged over 18 bond configurations. The parameters used were $U/t = 15.0113$ and $V_d/t = 10.0219$ for varying V_α , with $\alpha = b, p$, and q .

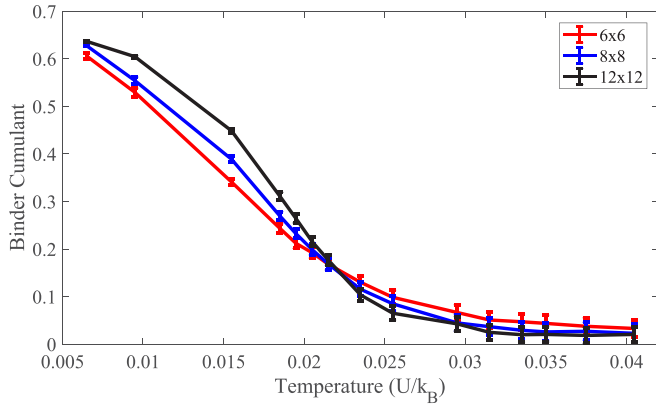


FIG. 13. Binder cumulant plot of $V_d/t = 10.0219$ for lattice sizes 6×6 , 8×8 , and 12×12 . Other parameters used are $U/t = 15.0113$, $V_b/t = 1.0547$, $V_p/t = 1.0623$, and $V_q/t = 1.0412$.

with $\pm J$ couplings, for which there are only four neighbors per site, that is a spin glass only at zero temperature [42,43].

We regard this paper as a proof of principle that glassiness can arise in models that are relevant for κ -(BEDT-TTF) $_2X$ salts and see future avenues for exploration through (i) studying a wider range of extended Hubbard model parameters, (ii) allowing for time-dependent couplings, and (iii) investigating the effects of quantum terms in the effective model. In addition to the equilibrium calculations considered here, the study of out-of-equilibrium dynamics in larger systems may help to determine the functional time dependence of aging dynamics that might also be accessible in experiments.

ACKNOWLEDGMENTS

The authors acknowledge Compute Canada resources that were used to obtain the numerical results in this paper. M.B.D. and M.P.K. were supported by Natural Sciences and Engineering Research Council.

APPENDIX A: COMMUTATORS USED IN THE STRONG-COUPLING EXPANSION

In this Appendix, we provide derivations of a number of commutators that prove useful in constructing the strong-coupling expansion of the Hamiltonian. Many of the commutators derived here have corresponding simpler versions in Ref. [32] in which the strong-coupling expansion was performed on a square lattice of sites rather than a triangular lattice of dimers.

1. Useful commutators

Before deriving the commutator $[H_0, T_\alpha^{m, \{M_2\}, \{M_1\}}]$, it is helpful to first derive a few basic commutators that are used in the derivation of the commutator of H_0 with the hopping operator. We begin with

$$[n_{(x,y),i,\sigma}, c_{(x',y'),j,\sigma'}^\dagger c_{(x'',y''),k,\sigma'}] = \delta_{\sigma,\sigma'} [\delta_{(x,y),(x',y')} \delta_{i,j} - \delta_{(x,y),(x'',y'')} \delta_{i,k}] c_{(x',y'),j,\sigma'}^\dagger c_{(x'',y''),k,\sigma'}. \quad (\text{A1})$$

Setting $(x'', y'') = (x', y')$, $k = j$ in this result, it follows directly that

$$[n_{(x,y),i,\sigma}, n_{(x',y'),j,\sigma'}] = 0, \quad (\text{A2})$$

which implies

$$[n_{(x,y),i,\sigma}, h_{(x',y'),j,\sigma'}] = \{n_{(x,y),i,\sigma}, O_{(x',y'),j}^\beta [\tilde{n}^\beta]\} = \{h_{(x,y),i,\sigma}, O_{(x',y'),j}^\beta [\tilde{n}^\beta]\} = 0. \quad (\text{A3})$$

The next set of commutators needed are those of the form $[n_{(x,y),i,\sigma'}, (T_\alpha^m)_{(x',y';x'',y''),j,k,\sigma}]$ which must be calculated independently for each $m = -1, 0, 1$. In general, they can be written as

$$[n_{(x,y),i,\sigma'}, (T_\alpha^m)_{(x',y';x'',y''),j,k,\sigma}] = (T_\alpha^m)_{(x',y';x'',y''),j,k,\sigma} \delta_{\sigma,\sigma'} [\delta_{(x,y),(x'',y'')} \delta_{i,k} - \delta_{(x,y),(x',y')} \delta_{i,j}]. \quad (\text{A4})$$

2. Onsite interaction commutator

Using Eq. (A4), one can show straightforwardly that, in general,

$$[H_U, T_\alpha^{m, \{M_2\}, \{M_1\}}] = m U T_\alpha^{m, \{M_2\}, \{M_1\}}. \quad (\text{A5})$$

3. Nearest neighbor interaction commutator

Before deriving the next commutator, it is useful to first rewrite the nearest neighbor interaction term as

$$H_V = \frac{1}{2} \sum_\gamma V_\gamma \sum_{(x,y)} \sum_{\substack{(\delta_{xy}, \delta_{yy}) \\ \delta_\gamma}} \sum_{\sigma, \sigma'} n_{(x,y),i,\sigma} n_{(x+\delta_{xy}, y+\delta_{yy}), i+\delta_\gamma, \sigma'}, \quad (\text{A6})$$

where $\gamma = d, q, b, p$ and the factor of $\frac{1}{2}$ is to prevent double counting. It is possible to further rewrite this as

$$H_V = \frac{1}{2} \sum_\gamma V_\gamma \sum_{(x,y)} \sum_\sigma n_{(x,y),i,\sigma} \tilde{n}_{(x,y),i}^\gamma, \quad (\text{A7})$$

where

$$\tilde{n}_{(x,y),i}^\gamma = \sum_{\substack{(\delta_{xy}, \delta_{yy}) \\ \delta_y}} \sum_{\bar{\sigma}} n_{(x+\delta_{xy}, y+\delta_{yy}), i+\delta_y, \bar{\sigma}}. \quad (\text{A8})$$

The desired commutator now takes the form:

$$\begin{aligned} [H_V, T_\alpha^{m, \{M_2\}, \{M_1\}}] &= \frac{1}{2} \sum_\gamma V_\gamma \sum_{\substack{(x,y) \\ i}} \sum_{\substack{(x',y') \\ j}} \sum'_{\substack{(x'',y'') \\ k}} \left\{ \prod_\beta \sum_{S[n_2^\beta]=M_2^\beta} \sum_{S[n_1^\beta]=M_1^\beta} \right\} \left\{ \prod_\eta O_{(x'',y''),k}^\eta [n_2^\eta] \right\} \\ &\quad \times \sum_{\sigma, \sigma'} [n_{(x,y),i,\sigma'} \tilde{n}_{(x,y),i}^\gamma, (T_\alpha^m)_{(x',y';x'',y''),j,k,\sigma}] \left\{ \prod_\xi O_{(x',y'),j}^\xi [n_1^\xi] \right\} \\ &= \frac{1}{2} \sum_\gamma V_\gamma \sum_{\substack{(x,y) \\ i}} \sum_{\substack{(x',y') \\ j}} \sum'_{\substack{(x'',y'') \\ k}} \left\{ \prod_\beta \sum_{S[n_2^\beta]=M_2^\beta} \sum_{S[n_1^\beta]=M_1^\beta} \right\} \left\{ \prod_\eta O_{(x'',y''),k}^\eta [n_2^\eta] \right\} \\ &\quad \times \sum_{\sigma, \sigma'} \left\{ n_{(x,y),i,\sigma'} [\tilde{n}_{(x,y),i}^\gamma, (T_\alpha^m)_{(x',y';x'',y''),j,k,\sigma}] \right. \\ &\quad \left. + [n_{(x,y),i,\sigma'}, (T_\alpha^m)_{(x',y';x'',y''),j,k,\sigma}] \tilde{n}_{(x,y),i}^\gamma \right\} \left\{ \prod_\xi O_{(x',y'),j}^\xi [n_1^\xi] \right\}. \quad (\text{A9}) \end{aligned}$$

Equation (A4) can then be used to obtain

$$\begin{aligned} &[\tilde{n}_{(x,y),i}^\gamma, (T_\alpha^m)_{(x',y';x'',y''),j,k,\sigma}] \\ &= \sum_{\substack{(\delta_{xy}, \delta_{yy}) \\ \delta_y}} \sum_{\bar{\sigma}} (T_\alpha^m)_{(x',y';x'',y''),j,k,\sigma} \delta_{\sigma, \bar{\sigma}} [\delta_{(x+\delta_{xy}, y+\delta_{yy}), (x'',y'') \delta_{i+\delta_y, k} - \delta_{(x+\delta_{xy}, y+\delta_{yy}), (x',y') \delta_{i+\delta_y, j}}]. \quad (\text{A10}) \end{aligned}$$

Applying Eq. (A4) and relabeling some indices leads to

$$\begin{aligned} [H_V, T_\alpha^{m, \{M_2\}, \{M_1\}}] &= \frac{1}{2} \sum_\gamma V_\gamma \sum_{\substack{(x',y') \\ j}} \sum'_{\substack{(x'',y'') \\ k}} \sum_\sigma \left\{ \prod_\beta \sum_{S[n_2^\beta]=M_2^\beta} \sum_{S[n_1^\beta]=M_1^\beta} \right\} \left\{ \prod_\eta O_{(x'',y''),k}^\eta [n_2^\eta] \right\} \\ &\quad \times \left\{ [\tilde{n}_{(x'',y''),k}^\gamma - \tilde{n}_{(x',y'),j}^\gamma] (T_\alpha^m)_{(x',y';x'',y''),j,k,\sigma} \right. \\ &\quad \left. + (T_\alpha^m)_{(x',y';x'',y''),j,k,\sigma} [\tilde{n}_{(x'',y''),k}^\gamma - \tilde{n}_{(x',y'),j}^\gamma] \right\} \left\{ \prod_\xi O_{(x',y'),j}^\xi [n_1^\xi] \right\}. \quad (\text{A11}) \end{aligned}$$

The central part of this equation can be rewritten as

$$\begin{aligned} &\tilde{n}_{(x'',y''),k}^\gamma (T_\alpha^m)_{(x',y';x'',y''),j,k,\sigma} - \tilde{n}_{(x',y'),j}^\gamma (T_\alpha^m)_{(x',y';x'',y''),j,k,\sigma} \\ &\quad + (T_\alpha^m)_{(x',y';x'',y''),j,k,\sigma} \tilde{n}_{(x'',y''),k}^\gamma - (T_\alpha^m)_{(x',y';x'',y''),j,k,\sigma} \tilde{n}_{(x',y'),j}^\gamma \\ &= 2[\tilde{n}_{(x'',y''),k}^\gamma (T_\alpha^m)_{(x',y';x'',y''),j,k,\sigma} - (T_\alpha^m)_{(x',y';x'',y''),j,k,\sigma} \tilde{n}_{(x',y'),j}^\gamma] \\ &\quad + [(T_\alpha^m)_{(x',y';x'',y''),j,k,\sigma}, \tilde{n}_{(x'',y''),k}^\gamma] - [\tilde{n}_{(x',y'),j}^\gamma, (T_\alpha^m)_{(x',y';x'',y''),j,k,\sigma}]. \quad (\text{A12}) \end{aligned}$$

When Eq. (A12) is inserted into Eq. (A11) and Eq. (A10) is also applied, this leads to the result

$$\begin{aligned} [H_V, T_\alpha^{m, \{M_2\}, \{M_1\}}] &= \sum_\gamma V_\gamma \sum_{\substack{(x',y') \\ j}} \sum'_{\substack{(x'',y'') \\ k}} \sum_\sigma \left\{ \prod_\beta \sum_{S[n_2^\beta]=M_2^\beta} \sum_{S[n_1^\beta]=M_1^\beta} \right\} \left\{ \prod_\eta O_{(x'',y''),k}^\eta [n_2^\eta] \right\} \\ &\quad \times [\tilde{n}_{(x'',y''),k}^\gamma (T_\alpha^m)_{(x',y';x'',y''),j,k,\sigma} - (T_\alpha^m)_{(x',y';x'',y''),j,k,\sigma} \tilde{n}_{(x',y'),j}^\gamma] \left\{ \prod_\xi O_{(x',y'),j}^\xi [n_1^\xi] \right\}. \quad (\text{A13}) \end{aligned}$$

and this becomes

$$[H_V, T_\alpha^{m, \{M_2\}, \{M_1\}}] = \sum_\gamma V_\gamma (M_2^\gamma - M_1^\gamma) T_\alpha^{m, \{M_2\}, \{M_1\}}, \quad (\text{A14})$$

which gives a commutator analogous to Eq. (A5).

APPENDIX B: DETAILS OF THE STRONG-COUPLING EXPANSION

In this Appendix, we write the decomposed hopping operator as

$$T_\alpha^{m, \{M_2\}, \{M_1\}} = Y_{m, \alpha}^{\{M_2\}, \{M_1\}}, \quad (\text{B1})$$

which satisfies the commutator

$$[H_0, Y_{m, \alpha}^{\{M_2\}, \{M_1\}}] = \epsilon_m^{\{M_2\}, \{M_1\}} Y_{m, \alpha}^{\{M_2\}, \{M_1\}}, \quad (\text{B2})$$

with $\epsilon_m^{\{M_2\}, \{M_1\}} = mU + \sum_\gamma V_\gamma (M_2^\gamma - M_1^\gamma)$ and $H_0 = H_U + H_V$. Recall that solutions for S_n and $H'_{T,n}$ are required such that Eq. (9) is satisfied to some desired order in $1/U$. For S_1 , we must solve

$$\{H_0, [S_1, \tilde{H}_0] + H_T\} = 0, \quad (\text{B3})$$

and remembering that $\tilde{H}_0 = H_0/U$, it is possible to rearrange this as

$$\begin{aligned} \{\tilde{H}_0, [\tilde{H}_0, S_1]\} &= [\tilde{H}_0, H_T] = \sum_{\substack{m, \alpha \\ \{M_2\}, \{M_1\}}} [\tilde{H}_0, Y_{m, \alpha}^{\{M_2\}, \{M_1\}}] \\ &= \sum_{\substack{m, \alpha \\ \{M_2\}, \{M_1\}}} \frac{\epsilon_m^{\{M_2\}, \{M_1\}}}{U} Y_{m, \alpha}^{\{M_2\}, \{M_1\}}. \end{aligned} \quad (\text{B4})$$

We can verify that S_1 takes the form:

$$S_1 = \sum_{\substack{m, \alpha \\ \{M_2\}, \{M_1\}}} \tilde{\sum} \frac{U}{\epsilon_m^{\{M_2\}, \{M_1\}}} Y_{m, \alpha}^{\{M_2\}, \{M_1\}}, \quad (\text{B5})$$

where the tilde over the sum indicates that all terms in the sum which have $\epsilon_m^{\{M_2\}, \{M_1\}} = 0$ are excluded. Substituting this into Eq. (B4) gives

$$\begin{aligned} \sum_{\substack{m, \alpha \\ \{M_2\}, \{M_1\}}} \tilde{\sum} \frac{U}{\epsilon_m^{\{M_2\}, \{M_1\}}} \left(\frac{\epsilon_m^{\{M_2\}, \{M_1\}}}{U} \right)^2 Y_{m, \alpha}^{\{M_2\}, \{M_1\}} \\ = \sum_{\substack{m, \alpha \\ \{M_2\}, \{M_1\}}} \frac{\epsilon_m^{\{M_2\}, \{M_1\}}}{U} Y_{m, \alpha}^{\{M_2\}, \{M_1\}}, \end{aligned} \quad (\text{B6})$$

and since it is possible to drop the $\epsilon_m^{\{M_2\}, \{M_1\}} = 0$ terms from the sum on the right-hand side with no consequence, this

becomes

$$\sum_{\substack{m, \alpha \\ \{M_2\}, \{M_1\}}} \tilde{\sum} \frac{\epsilon_m^{\{M_2\}, \{M_1\}}}{U} Y_{m, \alpha}^{\{M_2\}, \{M_1\}} = \sum_{\substack{m, \alpha \\ \{M_2\}, \{M_1\}}} \frac{\epsilon_m^{\{M_2\}, \{M_1\}}}{U} Y_{m, \alpha}^{\{M_2\}, \{M_1\}}, \quad (\text{B7})$$

verifying that the form of S_1 in Eq. (B5) solves Eq. (B4). Now that the form of S_1 is known, it is possible to calculate the form of the first-order correction:

$$\begin{aligned} H'_{T,1} &= H_T - [\tilde{H}_0, S_1] = \sum_{\substack{m, \alpha \\ \{M_2\}, \{M_1\}}} Y_{m, \alpha}^{\{M_2\}, \{M_1\}} \\ &\quad - \sum_{\substack{m, \alpha \\ \{M_2\}, \{M_1\}}} \tilde{\sum} \frac{U}{\epsilon_m^{\{M_2\}, \{M_1\}}} \frac{\epsilon_m^{\{M_2\}, \{M_1\}}}{U} Y_{m, \alpha}^{\{M_2\}, \{M_1\}} \\ &= \sum_{\substack{m, \alpha \\ \{M_2\}, \{M_1\}}} Y_{m, \alpha}^{\{M_2\}, \{M_1\}} - \sum_{\substack{m, \alpha \\ \{M_2\}, \{M_1\}}} \tilde{\sum} Y_{m, \alpha}^{\{M_2\}, \{M_1\}} \\ &= \sum_{\substack{m, \alpha \\ \{M_2\}, \{M_1\}}}^* Y_{m, \alpha}^{\{M_2\}, \{M_1\}}, \end{aligned} \quad (\text{B8})$$

where the star above the sum denotes that the sum only includes terms in which $\epsilon_m^{\{M_2\}, \{M_1\}} = 0$. In the hopping operator notation, this correction takes the form:

$$H'_{T,1} = \sum_\alpha \sum_{\substack{m \\ \{M_2\}, \{M_1\}}}^* T_\alpha^{m, \{M_2\}, \{M_1\}}. \quad (\text{B9})$$

Strictly, it is possible that the starred restriction is satisfied by having the $mU + \sum_\gamma V_\gamma (M_2^\gamma - M_1^\gamma)$ perfectly cancel for nonzero m , $\{M_1\}$ and $\{M_2\}$; however, if U and V_γ are chosen so that this is never the case, we will have $m = 0$, $\{M_2\} = \{M_1\}$, allowing the first-order correction to be written as

$$H'_{T,1} = \sum_\alpha \sum_{\{M\}} T_\alpha^{0, \{M\}, \{M\}}, \quad (\text{B10})$$

with no additional conditions, completing the first-order perturbation theory.

Before finding S_2 and the second-order correction, it is worthwhile to recall the Jacobi identity:

$$\{A, [B, C]\} + \{C, [A, B]\} + \{B, [C, A]\} = 0, \quad (\text{B11})$$

which we can use to write

$$\begin{aligned} \{\tilde{H}_0, [Y_{m, \alpha}^{\{M_2\}, \{M_1\}}, Y_{n, \nu}^{\{N_2\}, \{N_1\}}]\} \\ = \frac{\epsilon_m^{\{M_2\}, \{M_1\}} + \epsilon_n^{\{N_2\}, \{N_1\}}}{U} [Y_{m, \alpha}^{\{M_2\}, \{M_1\}}, Y_{n, \nu}^{\{N_2\}, \{N_1\}}]. \end{aligned} \quad (\text{B12})$$

TABLE II. Coefficients for $i = (x, y)$ and $j = (x \pm 1, y)$.

Coupling	$i = (x, y)$ $j = (x + 1, y)$	$i = (x, y)$ $j = (x - 1, y)$
$C_{i,j}^0$	$\frac{C_2}{2}$	$-\frac{C_2}{2}$
$C_{i,j}^1$	$-\frac{C_2}{2}$	$\frac{C_2}{2}$
$C_{i,j}^2$	$2C_1 - C_2$	$2C_1 - C_2$
$C_{i,j}^3$	$-C_2$	$-C_2$
$C_{i,j}^4$	$-2C_2$	$2C_2$
$C_{i,j}^5$	$2C_2$	$-2C_2$
$C_{i,j}^6$	$4C_2$	$4C_2$

For S_2 , we must solve

$$\begin{aligned}
\{\tilde{H}_0, [\tilde{H}_0, S_2]\} &= \frac{1}{2}(\tilde{H}_0, \{S_1, [S_1, \tilde{H}_0]\}) + \{\tilde{H}_0, [S_1, H_T]\} \\
&= -\sum_{\substack{m,\alpha \\ \{M_2\}, \{M_1\}}} \tilde{\sum}_{\substack{n,v \\ \{N_2\}, \{N_1\}}} \frac{\epsilon_m^{\{M_2\}, \{M_1\}} + \epsilon_n^{\{N_2\}, \{N_1\}}}{2\epsilon_m^{\{M_2\}, \{M_1\}}} \\
&\quad \times [Y_{m,\alpha}^{\{M_2\}, \{M_1\}}, Y_{n,v}^{\{N_2\}, \{N_1\}}] \\
&\quad + \sum_{\substack{m,\alpha \\ \{M_2\}, \{M_1\}}} \tilde{\sum}_{\substack{n,v \\ \{N_2\}, \{N_1\}}} \frac{\epsilon_m^{\{M_2\}, \{M_1\}} + \epsilon_n^{\{N_2\}, \{N_1\}}}{\epsilon_m^{\{M_2\}, \{M_1\}}} \\
&\quad \times [Y_{m,\alpha}^{\{M_2\}, \{M_1\}}, Y_{n,v}^{\{N_2\}, \{N_1\}}], \quad (\text{B13})
\end{aligned}$$

where we used Eq. (B12) in Eq. (B13). It is possible to rewrite

$$\sum_{\substack{n,v \\ \{N_2\}, \{N_1\}}} = \tilde{\sum}_{\substack{n,v \\ \{N_2\}, \{N_1\}}} + \sum_{\substack{n,v \\ \{N_2\}, \{N_1\}}}^*, \quad (\text{B14})$$

by breaking up the sum into parts which have $\epsilon_n^{\{N_2\}, \{N_1\}} \neq 0$ and parts which have $\epsilon_n^{\{N_2\}, \{N_1\}} = 0$. The commutator equation then becomes

$$\begin{aligned}
\{\tilde{H}_0, [\tilde{H}_0, S_2]\} &= \sum_{\substack{m,\alpha \\ \{M_2\}, \{M_1\}}} \tilde{\sum}_{\substack{n,v \\ \{N_2\}, \{N_1\}}} \frac{\epsilon_m^{\{M_2\}, \{M_1\}} + \epsilon_n^{\{N_2\}, \{N_1\}}}{2\epsilon_m^{\{M_2\}, \{M_1\}}} \\
&\quad \times [Y_{m,\alpha}^{\{M_2\}, \{M_1\}}, Y_{n,v}^{\{N_2\}, \{N_1\}}] \\
&\quad + \sum_{\substack{m,\alpha \\ \{M_2\}, \{M_1\}}} \sum_{\substack{n,v \\ \{N_2\}, \{N_1\}}}^* \frac{\epsilon_m^{\{M_2\}, \{M_1\}} + 0}{\epsilon_m^{\{M_2\}, \{M_1\}}} \\
&\quad \times [Y_{m,\alpha}^{\{M_2\}, \{M_1\}}, Y_{n,v}^{\{N_2\}, \{N_1\}}]. \quad (\text{B15})
\end{aligned}$$

Dropping the $\epsilon_m^{\{M_2\}, \{M_1\}} + \epsilon_n^{\{N_2\}, \{N_1\}} = 0$ terms from the first summation has no consequence, allowing this to be written as

$$\begin{aligned}
\{\tilde{H}_0, [\tilde{H}_0, S_2]\} &= \overline{\sum}_{\substack{m,\alpha \\ \{M_2\}, \{M_1\}}} \overline{\sum}_{\substack{n,v \\ \{N_2\}, \{N_1\}}} \frac{\epsilon_m^{\{M_2\}, \{M_1\}} + \epsilon_n^{\{N_2\}, \{N_1\}}}{2\epsilon_m^{\{M_2\}, \{M_1\}}} \\
&\quad \times [Y_{m,\alpha}^{\{M_2\}, \{M_1\}}, Y_{n,v}^{\{N_2\}, \{N_1\}}] \\
&\quad + \sum_{\substack{m,\alpha \\ \{M_2\}, \{M_1\}}} \sum_{\substack{n,v \\ \{N_2\}, \{N_1\}}}^* [Y_{m,\alpha}^{\{M_2\}, \{M_1\}}, Y_{n,v}^{\{N_2\}, \{N_1\}}], \quad (\text{B16})
\end{aligned}$$

where the overbar indicates that the sums exclude all terms which have $\epsilon_m^{\{M_2\}, \{M_1\}} = 0$, $\epsilon_n^{\{N_2\}, \{N_1\}} = 0$, and $\epsilon_m^{\{M_2\}, \{M_1\}} + \epsilon_n^{\{N_2\}, \{N_1\}} = 0$. Again, rather than solving this equation explicitly for S_2 , a solution of the form

$$\begin{aligned}
S_2 &= \overline{\sum}_{\substack{m,\alpha \\ \{M_2\}, \{M_1\}}} \overline{\sum}_{\substack{n,v \\ \{N_2\}, \{N_1\}}} \frac{U^2}{2\epsilon_m^{\{M_2\}, \{M_1\}} (\epsilon_m^{\{M_2\}, \{M_1\}} + \epsilon_n^{\{N_2\}, \{N_1\}})} \\
&\quad \times [Y_{m,\alpha}^{\{M_2\}, \{M_1\}}, Y_{n,v}^{\{N_2\}, \{N_1\}}] \\
&\quad + \sum_{\substack{m,\alpha \\ \{M_2\}, \{M_1\}}} \sum_{\substack{n,v \\ \{N_2\}, \{N_1\}}}^* \left(\frac{U}{\epsilon_m^{\{M_2\}, \{M_1\}}} \right)^2 [Y_{m,\alpha}^{\{M_2\}, \{M_1\}}, Y_{n,v}^{\{N_2\}, \{N_1\}}] \quad (\text{B17})
\end{aligned}$$

can be guessed and easily verified by substitution into Eq. (B16). Now that both S_1 and S_2 are known, it is possible to calculate the second-order correction

$$\begin{aligned}
H'_{T,2} &= [S_1, H_T] + \frac{1}{2}\{S_1, [S_1, \tilde{H}_0]\} + [S_2, \tilde{H}_0] \\
&= \sum_{\substack{m,\alpha \\ \{M_2\}, \{M_1\}}} \tilde{\sum}_{\substack{n,v \\ \{N_2\}, \{N_1\}}} \frac{U}{\epsilon_m^{\{M_2\}, \{M_1\}}} [Y_{m,\alpha}^{\{M_2\}, \{M_1\}}, Y_{n,v}^{\{N_2\}, \{N_1\}}] \\
&\quad - \sum_{\substack{m,\alpha \\ \{M_2\}, \{M_1\}}} \tilde{\sum}_{\substack{n,v \\ \{N_2\}, \{N_1\}}} \frac{U}{2\epsilon_m^{\{M_2\}, \{M_1\}}} [Y_{m,\alpha}^{\{M_2\}, \{M_1\}}, Y_{n,v}^{\{N_2\}, \{N_1\}}] \\
&\quad - \sum_{\substack{m,\alpha \\ \{M_2\}, \{M_1\}}} \overline{\sum}_{\substack{n,v \\ \{N_2\}, \{N_1\}}} \frac{U}{2\epsilon_m^{\{M_2\}, \{M_1\}}} [Y_{m,\alpha}^{\{M_2\}, \{M_1\}}, Y_{n,v}^{\{N_2\}, \{N_1\}}] \\
&\quad - \sum_{\substack{m,\alpha \\ \{M_2\}, \{M_1\}}} \sum_{\substack{n,v \\ \{N_2\}, \{N_1\}}}^* \frac{U}{\epsilon_m^{\{M_2\}, \{M_1\}}} [Y_{m,\alpha}^{\{M_2\}, \{M_1\}}, Y_{n,v}^{\{N_2\}, \{N_1\}}], \quad (\text{B18})
\end{aligned}$$

and using Eq. (B14) to break up the sum leads directly to

$$\begin{aligned}
H'_{T,2} &= \tilde{\sum}_{\substack{m,\alpha \\ \{M_2\}, \{M_1\}}} \tilde{\sum}_{\substack{n,v \\ \{N_2\}, \{N_1\}}} \frac{U}{2\epsilon_m^{\{M_2\}, \{M_1\}}} [Y_{m,\alpha}^{\{M_2\}, \{M_1\}}, Y_{n,v}^{\{N_2\}, \{N_1\}}] \\
&\quad - \sum_{\substack{m,\alpha \\ \{M_2\}, \{M_1\}}} \overline{\sum}_{\substack{n,v \\ \{N_2\}, \{N_1\}}} \frac{U}{2\epsilon_m^{\{M_2\}, \{M_1\}}} [Y_{m,\alpha}^{\{M_2\}, \{M_1\}}, Y_{n,v}^{\{N_2\}, \{N_1\}}], \quad (\text{B19})
\end{aligned}$$

which can be simplified to

$$H'_{T,2} = \overline{\overline{\sum}_{\substack{m,\alpha \\ \{M_2\}, \{M_1\}}} \sum_{\substack{n,v \\ \{N_2\}, \{N_1\}}} \frac{U}{\epsilon_m^{\{M_2\}, \{M_1\}}} Y_{m,\alpha}^{\{M_2\}, \{M_1\}} Y_{n,v}^{\{N_2\}, \{N_1\}}}, \quad (\text{B20})$$

where the double overbar indicates that the sums include only terms which satisfy $\epsilon_m^{\{M_2\}, \{M_1\}} + \epsilon_n^{\{N_2\}, \{N_1\}} = 0$, $\epsilon_m^{\{M_2\}, \{M_1\}} \neq 0$, $\epsilon_n^{\{N_2\}, \{N_1\}} \neq 0$. To simplify this further, it is necessary to go back to the full hopping operator notation, in which case:

$$H'_{T,2} = U \sum_{\alpha,v} \overline{\overline{\sum}_{\substack{\{M_2\}, \{M_1\} \\ \{N_2\}, \{N_1\}}} \sum_{m,n} \frac{T_\alpha^{m, \{M_2\}, \{M_1\}} T_v^{n, \{N_2\}, \{N_1\}}}{mU + \sum_\gamma V_\gamma (M_2^\gamma - M_1^\gamma)}}. \quad (\text{B21})$$

Now, for the double overbar restriction to be satisfied for all U and V_γ , the only terms that will be in the sum are those

TABLE III. Coefficients for $i = (x, y)$ and $j = (x + \frac{1}{2}, y - \frac{1}{2})$ or $j = (x - \frac{1}{2}, y + \frac{1}{2})$.

Coupling	$i = (x, y)$ and $j = (x + \frac{1}{2}, y - \frac{1}{2})$	$i = (x, y)$ and $j = (x - \frac{1}{2}, y + \frac{1}{2})$
$C_{i,j}^0$	$\frac{1}{2}(C_7 - C_8)$	$-\frac{1}{2}(C_7 - C_8)$
$C_{i,j}^1$	$\frac{1}{2}(C_7 + C_8)$	$-\frac{1}{2}(C_7 + C_8)$
$C_{i,j}^2$	$2(C_6 - C_5) + (C_7 - C_8)$	$2(C_6 - C_5) - (C_7 - C_8)$
$C_{i,j}^3$	$-(C_7 + C_8)$	$-(C_7 + C_8)$
$C_{i,j}^4$	$2(C_8 - C_7)$	$2(C_7 - C_8)$
$C_{i,j}^5$	$-2(C_7 + C_8)$	$2(C_7 + C_8)$
$C_{i,j}^6$	$4(C_8 - C_7)$	$-4(C_7 - C_8)$
$C_{i,j}^7$	$\frac{1}{4}(3C_3 + C_4)$	$\frac{1}{4}(3C_3 + C_4)$
$C_{i,j}^8$	$-\frac{1}{2}(C_3 - C_4)$	$\frac{1}{2}(C_3 - C_4)$
$C_{i,j}^9$	$C_3 - C_4$	$C_3 - C_4$
$C_{i,j}^{10}$	$2(C_3 - C_4)$	$-2(C_3 - C_4)$

TABLE IV. Coefficients for $i = (x, y)$ and $j = (x + \frac{1}{2}, y + \frac{1}{2})$ or $j = (x - \frac{1}{2}, y - \frac{1}{2})$.

Coupling	$i = (x, y)$ and $j = (x + \frac{1}{2}, y + \frac{1}{2})$	$i = (x, y)$ and $j = (x - \frac{1}{2}, y - \frac{1}{2})$
$C_{i,j}^0$	$\frac{1}{2}(C_7 + C_8)$	$-\frac{1}{2}(C_7 + C_8)$
$C_{i,j}^1$	$\frac{1}{2}(C_7 - C_8)$	$-\frac{1}{2}(C_7 - C_8)$
$C_{i,j}^2$	$2(C_6 - C_5) + (C_7 - C_8)$	$2(C_6 - C_5) + (C_7 - C_8)$
$C_{i,j}^3$	$-(C_7 + C_8)$	$-(C_7 + C_8)$
$C_{i,j}^4$	$-2(C_7 + C_8)$	$2(C_7 + C_8)$
$C_{i,j}^5$	$-2(C_7 - C_8)$	$2(C_7 - C_8)$
$C_{i,j}^6$	$-4(C_7 + C_8)$	$-4(C_7 - C_8)$
$C_{i,j}^{11}$	$\frac{1}{4}(3C_3 + C_4)$	$\frac{1}{4}(3C_3 + C_4)$
$C_{i,j}^{12}$	$\frac{1}{2}(C_2 - C_3)$	$\frac{1}{2}(C_3 - C_4)$
$C_{i,j}^{13}$	$C_3 - C_2$	$C_3 - C_4$
$C_{i,j}^{14}$	$2(C_3 - C_2)$	$-2(C_3 - C_4)$

that have $n = -m$, $\{N_1\} = \{M_2\} - \{M_1\} + \{N_2\}$, which allows $H'_{T,2}$ to be reduced to

$$H'_{T,2} = U \sum_{\alpha, \nu} \sum_{\substack{\{M_2\}, \{M_1\} \\ \{N\}, m}} \frac{T_{\alpha}^{m, \{M_2\}, \{M_1\}} T_{\nu}^{-m, \{N\}, \{M_2\} - \{M_1\} + \{N\}}}{mU + \sum_{\gamma} V_{\gamma} (M_2^{\gamma} - M_1^{\gamma})}, \quad (\text{B22})$$

$$\begin{aligned} C_1 &= \frac{t_b^2}{\sum_{\gamma} V_{\gamma} (M_2^{\gamma} - M_1^{\gamma})}, & C_2 &= \frac{t_b^2}{-U + \sum_{\gamma} V_{\gamma} (M_2^{\gamma} - M_1^{\gamma})}, \\ C_3 &= \frac{t_p t_q}{\sum_{\gamma} V_{\gamma} (M_2^{\gamma} - M_1^{\gamma})}, & C_4 &= \frac{t_q t_p}{-U + \sum_{\gamma} V_{\gamma} (M_2^{\gamma} - M_1^{\gamma})}, \\ C_5 &= \frac{t_q^2}{\sum_{\gamma} V_{\gamma} (M_2^{\gamma} - M_1^{\gamma})}, & C_6 &= \frac{t_p^2}{\sum_{\gamma} V_{\gamma} (M_2^{\gamma} - M_1^{\gamma})}, \\ C_7 &= \frac{t_q^2}{-U + \sum_{\gamma} V_{\gamma} (M_2^{\gamma} - M_1^{\gamma})}, & C_8 &= \frac{t_p^2}{-U + \sum_{\gamma} V_{\gamma} (M_2^{\gamma} - M_1^{\gamma})}. \end{aligned}$$

1. Tables of coefficients

In Tables II–IV, we set out the relationships between the coefficients C_1 – C_8 listed above and the coefficients that enter

with no additional conditions, which completes the second-order perturbation theory.

APPENDIX C: SECOND-ORDER PROCESSES AND CONTRIBUTIONS

There are eight different types of second-order processes, each of which is associated with a particular coupling. We list each of the eight couplings C_n , with $n = 1$ – 8 , along with an illustrative example for each coupling in Table I, where

the effective model Eq. (27). The coefficients vary for each type of pair of dimers. We only list nonzero coefficients.

- [1] B. J. Powell and R. H. McKenzie, *Rep. Prog. Phys.* **74**, 056501 (2011).
- [2] C. Hotta, *Crystals* **2**, 1155 (2012).
- [3] M. Dressel and S. Tomić, *Adv. Phys.* **69**, 1 (2020).
- [4] Y. Shimizu, K. Miyagawa, K. Kanoda, M. Maesato, and G. Saito, *Phys. Rev. Lett.* **91**, 107001 (2003).

- [5] B. J. Powell and R. H. McKenzie, *J. Phys.: Condens. Matter* **18**, R827 (2006).
- [6] P. Lunkenheimer and A. Loidl, *J. Phys.: Condens. Matter* **27**, 373001 (2015).
- [7] S. Tomić and M. Dressel, *Rep. Prog. Phys.* **78**, 096501 (2015).

- [8] M. Abdel-Jawad, I. Terasaki, T. Sasaki, N. Yoneyama, N. Kobayashi, Y. Uesu, and C. Hotta, *Phys. Rev. B* **82**, 125119 (2010).
- [9] M. Pinterić, D. Rivas Góngora, Z. Rapljenović, T. Ivek, M. Čulo, B. Korin-Hamzić, O. Milat, B. Gumhalter, P. Lazić, M. Sanz Alonso *et al.*, *Crystals* **8**, 190 (2018).
- [10] M. Hemmida, H.-A. Krug von Nidda, B. Miksch, L. L. Samoilenko, A. Pustogow, S. Widmann, A. Henderson, T. Siegrist, J. A. Schlueter, A. Loidl *et al.*, *Phys. Rev. B* **98**, 241202(R) (2018).
- [11] N. Drichko, R. Beyer, E. Rose, M. Dressel, J. A. Schlueter, S. A. Turunova, E. I. Zhilyaeva, and R. N. Lyubovskaya, *Phys. Rev. B* **89**, 075133 (2014).
- [12] K. Sedlmeier, S. Elsässer, D. Neubauer, R. Beyer, D. Wu, T. Ivek, S. Tomić, J. A. Schlueter, and M. Dressel, *Phys. Rev. B* **86**, 245103 (2012).
- [13] M. Pinterić, M. Čulo, O. Milat, M. Basletić, B. Korin-Hamzić, E. Tafra, A. Hamzić, T. Ivek, T. Peterseim, K. Miyagawa *et al.*, *Phys. Rev. B* **90**, 195139 (2014).
- [14] H. Fukuyama, J.-I. Kishine, and M. Ogata, *J. Phys. Soc. Jpn.* **86**, 123706 (2017).
- [15] A. Pustogow, R. Rösslhuber, Y. Tan, E. Uykur, A. Böhme, M. Wenzel, Y. Saito, A. Löhle, R. Hübner, A. Kawamoto *et al.*, *npj Quantum Mater.* **6**, 9 (2021).
- [16] D. Guterding, R. Valenti, and H. O. Jeschke, *Phys. Rev. B* **92**, 081109(R) (2015).
- [17] B. Hartmann, D. Zielke, J. Polzin, T. Sasaki, and J. Müller, *Phys. Rev. Lett.* **114**, 216403 (2015).
- [18] J. Müller, B. Hartmann, R. Rommel, J. Brandenburg, S. M. Winter, and J. A. Schlueter, *New J. Phys.* **17**, 083057 (2015).
- [19] M. Abdel-Jawad, N. Tajima, R. Kato, and I. Terasaki, *Phys. Rev. B* **88**, 075139 (2013).
- [20] S. Fujiyama and R. Kato, *Phys. Rev. B* **97**, 035131 (2018).
- [21] S. Iguchi, S. Sasaki, N. Yoneyama, H. Taniguchi, T. Nishizaki, and T. Sasaki, *Phys. Rev. B* **87**, 075107 (2013).
- [22] J. Müller, S. Iguchi, H. Taniguchi, and T. Sasaki, *Phys. Rev. B* **102**, 100103(R) (2020).
- [23] F. Kagawa, T. Sato, K. Miyagawa, K. Kanoda, Y. Tokura, K. Kobayashi, R. Kumai, and Y. Murakami, *Nat. Phys.* **9**, 419 (2013).
- [24] T. Sato, F. Kagawa, K. Kobayashi, K. Miyagawa, K. Kanoda, R. Kumai, Y. Murakami, and Y. Tokura, *Phys. Rev. B* **89**, 121102(R) (2014).
- [25] T. Sato, K. Miyagawa, and K. Kanoda, *J. Phys. Soc. Jpn.* **85**, 123702 (2016).
- [26] P. Lunkenheimer, B. Hartmann, M. Lang, J. Müller, D. Schweitzer, S. Krohns, and A. Loidl, *Phys. Rev. B* **91**, 245132 (2015).
- [27] T. Ivek, M. Čulo, M. Kuveždić, E. Tutiš, M. Basletić, B. Mihaljević, E. Tafra, S. Tomić, A. Löhle, M. Dressel *et al.*, *Phys. Rev. B* **96**, 075141 (2017).
- [28] C. Hotta, *Phys. Rev. B* **82**, 241104(R) (2010).
- [29] M. Naka and S. Ishihara, *J. Phys. Soc. Jpn.* **79**, 063707 (2010).
- [30] H. Gomi, M. Ikenaga, Y. Hiragi, D. Segawa, A. Takahashi, T. J. Inagaki, and M. Aihara, *Phys. Rev. B* **87**, 195126 (2013).
- [31] J. Merino, H. Seo, and M. Ogata, *Phys. Rev. B* **71**, 125111 (2005).
- [32] A. Farrell, Topological Superconductivity without Proximity Effect, Master's thesis, McGill University, 2013.
- [33] A. Farrell and T. Pereg-Barnea, *Phys. Rev. B* **89**, 035112 (2014).
- [34] H. C. Kandpal, I. Opahle, Y.-Z. Zhang, H. O. Jeschke, and R. Valenti, *Phys. Rev. Lett.* **103**, 067004 (2009).
- [35] K. Nakamura, Y. Yoshimoto, T. Kosugi, R. Arita, and M. Imada, *J. Phys. Soc. Jpn.* **78**, 083710 (2009).
- [36] K. Nakamura, Y. Yoshimoto, and M. Imada, *Phys. Rev. B* **86**, 205117 (2012).
- [37] A. H. MacDonald, S. M. Girvin, and D. T. Yoshioka, *Phys. Rev. B* **37**, 9753 (1988).
- [38] M. Guo, R. N. Bhatt, and D. A. Huse, *Phys. Rev. B* **54**, 3336 (1996).
- [39] S. Franz and J. Hertz, *Phys. Rev. Lett.* **74**, 2114 (1995).
- [40] M. P. Kennett, C. Chamon, and L. F. Cugliandolo, *Phys. Rev. B* **72**, 024417 (2005).
- [41] L. Berthier, P. C. W. Holdsworth, and M. Sellitto, *J. Phys. A: Math. Gen.* **34**, 1805 (2001).
- [42] R. R. P. Singh and S. Chakravarty, *Phys. Rev. Lett.* **57**, 245 (1986).
- [43] R. N. Bhatt and A. P. Young, *Phys. Rev. B* **37**, 5606 (1988).